2014 年 8 月

碩士學位論文

흡수식 시스템의 판형열교환기에서 나노유체를 이용한 열전달 성능에 관한 해석적 연구

朝鮮大學校 大學院

機 械 工 學 科

陳 挺

흡수식 시스템의 판형열교환기에서 나노유체를 이용한 열전달 성능에 관한 해석적 연구

Simulation study on the heat transfer performance of LiBr solution based binary nanofluid in a PHE of an absorption system

2014年 8月 日

朝鮮大學校 大學院

機 械 工 學 科

陳 挺

흡수식 시스템의 판형열교환기에서 나노유체를 이용한 열전달 성능에 관한 해석적 연구

指導敎授 : 曺 弘 鉉

이 논문을 공학석사 학위신청 논문으로 제출함

2014 年 4 月

朝鮮大學校 大學院

機 械 工 學 科

陳 挺

陳挺의 碩士學位 論文을 認准함

委員長 朝鮮大學校 敎 授 洪 明 錫 ㊞

委 員 朝鮮大學校 敎 授 曺 弘 鉉 ㊞

委 員 朝鮮大學校 敎 授 金 志 勳 ㊞

2014 年 5 月

朝 鮮 大 學 校 大 學 院

Contents

Contents ····· i
List of Figures ····· iv
List of Tables ····· vi
Nomenclature ····· vii
ABSTRACT ····· x

Ⅰ. Introduction ····· 1
A. Background ····· 1
B. Previous studies ····· 2
C. Objectives ····· 6

Ⅱ. Modeling and verification ····· 7
A. Development of formulas for LiBr properties ····· 7
B. Verification of the proposed equations ····· 11
C. Nanofluid simulation ····· 14
D. Heat transfer performance analysis ····· 18

Ⅲ. Results and discussion ····· 19
A. Heat transfer characteristics of the PHE and verification of LiBr solution properties ····· 19
1. Heat transfer performance with varying mass flow rate of hot fluid ····· 19
a. Variation of heat transfer rate ····· 19

b. variation of overall heat transfer coefficient ·····21
c. Variation of effectiveness of PHE ·····23
2. Heat transfer performance with varying mass flow rate of cold fluid ·····25
a. Variation of heat transfer rate ·····25
b. variation of overall heat transfer coefficient ·····27
B. Analysis of the heat transfer performance of the PHE using Al_2O_3- nanofluid ·····28
1. Heat transfer performance with varying mass flow rate of hot fluid ·····28
a. Variation of heat transfer rate ·····28
b. variation of overall heat transfer coefficient ·····31
c. Variation of effectiveness and heat capacity rate ratio ·····33
2. Heat transfer performance with varying mass flow rate of cold fluid ·····36
a. Variation of heat transfer rate ·····36
b. Variation of effectiveness and heat capacity rate ratio ·····38
C. Analysis of the heat transfer performance of the PHE using Cu-nanofluid ·····40
1. Analysis of heat transfer rate ·····40
2. Analysis of heat transfer coefficient ·····42
3. Analysis of effectiveness of PHE ·····44
D. Analysis of the heat transfer performance of the PHE using MWCNT-nanofluid ·····46
1. Analysis of heat transfer rate ·····46

2. Analysis of heat transfer coefficient ·····48
3. Analysis of effectiveness of PHE ·····50
E. Comparison of the heat transfer performance of the PHE with different nanofluids ·····52
1. Comparison of heat transfer rate ·····52
2. Comparison of heat transfer coefficient ·····54
3. Comparison of effectiveness of PHE ·····56

Ⅳ Conclusion ·····57

REFERENCE ·····60

List of Figures

Fig. 1.1 Different kinds of chevron plate ····· 2

Fig. 2.1 Density of LiBr solution ····· 9

Fig. 2.2 Specific heat capacity of LiBr solution ····· 9

Fig. 2.3 Surface fitting for LiBr solution density ····· 10

Fig. 2.4 Surface fitting for LiBr solution specific heat capacity ····· 10

Fig. 2.5 Schematic of chevron plate ····· 23

Fig. 3.1 Comparison of experimental and computational heat transfer rate with mass flow rate of hot fluid ····· 20

Fig. 3.2 Comparison of experimental and computational overall heat transfer coefficient with mass flow rate of hot fluid ····· 22

Fig. 3.3 Comparison of experimental and computational effectiveness of the PHE with mass flow rate of hot fluid ····· 24

Fig. 3.4 Simulation results of heat transfer rate and effectiveness of the PHE with mass flow rate of cold fluid ····· 26

Fig. 3.5 Simulation results of heat transfer coefficient with mass flow rate of cold fluid ····· 27

Fig. 3.6 Variation of heat transfer rate for various Al_2O_3-nanofluids concentrations with mass flow rate of hot fluid ····· 30

Fig. 3.7 Variation of heat transfer coefficient for various Al_2O_3-nanofluids concentrations with mass flow rate of hot fluid ····· 32

Fig. 3.8 Variation of effectiveness of the PHE for various Al_2O_3-nanofluids

concentrations with mass flow rate of hot fluid ····· 35
Fig. 3.9 Variation of heat capacity rate ratio for various Al_2O_3-nanofluids concentrations with mass flow rate of hot fluid ····· 35
Fig. 3.10 Variation of heat transfer rate for various Al_2O_3-nanofluids concentrations with mass flow rate of cold fluid ····· 37
Fig. 3.11 Variation of effectiveness of the PHE for various Al_2O_3-nanofluids concentrations with mass flow rate of cold fluid ····· 38
Fig. 3.12 Variation of heat capacity rate ratio for various Al_2O_3-nanofluids concentrations with mass flow rate of cold fluid ····· 39
Fig. 3.13 Variation of heat transfer rate for various Cu-nanofluids concentrations with mass flow rate of hot fluid ····· 41
Fig. 3.14 Variation of heat transfer coefficient for various Cu-nanofluids concentrations with mass flow rate of hot fluid ····· 43
Fig. 3.15 Variation of effectiveness for various Cu-nanofluids concentrations with mass flow rate of hot fluid ····· 45
Fig. 3.16 Variation of heat transfer rate for various MWCNT-nanofluids concentrations with mass flow rate of hot fluid ····· 47
Fig. 3.17 Variation of heat transfer coefficient for various MWCNT-nanofluids concentrations with mass flow rate of hot fluid ····· 49
Fig. 3.18 Variation of effectiveness for various MWCNT-nanofluids concentrations with mass flow rate of hot fluid ····· 51
Fig. 3.19 Comparison of heat transfer rate for different optimal nanofluids with mass flow rate of hot fluid ····· 53
Fig. 3.20 Comparison of heat transfer coefficient for different optimal nanofluids with mass flow rate of hot fluid ····· 55

Fig. 3.21 Comparison of effectiveness of PHE for different optimal nanofluids with mass flow rate of hot fluid ····· 56

List of Tables

Table 2.1 Specification of chevron plate ·····12

Table 2.2 Test and simulation conditions of working fluid ·····13

Table 2.3 Thermophysical properties of nanoparticles ·····13

Nomenclature

A	: area, m^2
Cp	: heat capacity, kJ /kg·K
b	: corrugation depth, mm
c	: concentration, %
h	: heat transfer coefficient, $kW/m^2 \cdot ℃$
k	: conductivity, kW/m·K
Nu	: Nusselt number
Re	: Reynolds number
PHE	: plate heat exchanger
Pr	: Prandtl number
Q	: heat transfer rate, kW
ΔT	: temperature difference, ℃
U	: overall heat transfer coefficient, $kW/m^2 \cdot ℃$
T	: temperature, ℃
C*	: heat capacity rate ratio
t	: thickness, mm
M	: mass flow rate, kg/h

Greeks

μ	: viscosity
v	: volume fraction
ρ	: density, kg/m^3

β	: chevron angle
λ	: corrugation pitch, mm
ε	: effectiveness

Subscripts

nf	: nanofluid
bf	: basic fluid
p	: nanoparticle
h	: hot-fluid side
c	: cold-fluid side
m	: metal plate
i	: inlet
o	: outlet
min	: minimum
max	: maximum

초록

흡수식 시스템의 판형열교환기에서 나노유체를 이용한 열전달 성능에 관한 해석적 연구

진 정
지 도 교 수: 조 홍 현
조선대학교 기계공학과 대학원

본 논문에서는 판형 열교환기의 다양한 쉐브론 각도 및 질량유량과 함께 나노입자의 유무에 따른 LiBr 용액의 성능을 조사하였다. 본 연구에서는 Al_2O_3, Cu, 및 MWCNT를 나노입자로 사용하였으며, 나노 입자의 농도는 0.05vol.%~0.24vol.%로 변화시키며 진행하였다. 결과적으로, Al_2O_3 나노유체 의 경우, $60^o/60^o$ 쉐브론 각도의 열교환기의 열전달율, 총괄 열전달계수, 유용도는 $30^o/30^o$ 쉐브론 각도의 열교환기보다 각각 100%, 50%, 70% 정도 높게 나타났다. 동일한 조건에서 Al_2O_3 나노유체의 농도 변화에서는 3vol.%의 Al_2O_3 나노유체가 가장 높은 열전달율과 총괄 열전달계수를 나타내었다. Cu 나노유체 의 경우, 동일한 조건에서 $30^o/30^o$ 쉐브론 각도의 판형열교환기에서 나노입자의 농도를 변화시켰으며, 2vol.% 농도의 Cu 나노유체에서 가장 높은 열전달율과 유용도를 나타내었다. 또한, $30^o/60^o$ 와 $60^o/60^o$ 의 쉐브론 각도의 판형열교환기에서 나노유체의 농도변화는 4vol.% 의 농도에서 가장 높은 열전달율과 유용도를 나타났다. MWCNT 나노유체 의 경우, 안정성의 요인으로 체적 분율은 0.24vol.%를 초과할 수 없다. MWCNT 나노유체의 농도변화에서는 0.24vol.% MWCNT 나노유체가 가장 높은 열전달 성능을 나타내었다.

I. Introduction

A. Background

Since the invention of the plate heat exchanger (PHE) in 1921 for use in the dairy industry, it has been widely used in various fields. It consists of a set of thin, usually metal plates and a frame to support the plates. The working fluid flows through the gap between two adjacent plates. The heat transfer surface can be easily changed by adding or removing plates, and the heat transfer capacity can be adjusted within a certain range. With increasing demands for energy savings, the PHE now plays an increasingly important role in industry. A high efficiency PHE can substantially reduce energy waste.

There are several types of PHEs, such as chevron, herringbone, and wash board. Among these, the chevron PHE is the most widely used. Normally, a chevron plate can provide relatively high turbulence, enabling effective heat transfer. Heat transfer coefficients produced by a chevron PHE can be equal to values for tubes in which Reynolds numbers are five times higher according to Troupe (1960). For this reason, much research on chevron PHEs with different chevron angles has been conducted.

Changing the plate structure is one way to improve the heat transfer rate of a heat exchanger. However, it is difficult to develop a new type of PHE by changing the shape of the plate. Thus, researchers all over the world are attempting to find other ways to improve the heat exchange rate. Many industrial processes involve heat transfer by means of a flowing fluid in either the laminar or turbulent regime. Most of these processes are operated under a large range of

temperatures and pressures. Thus, high reliable devices are needed and companies have to cost more capitals. Many of them would benefit from a decrease in the thermal resistance of the working fluid. This kind of decrease in thermal resistance would lead to smaller heat transfer systems with lower capital costs and improved energy efficiencies. Nanofluids is exactly this kind of working fluid. Although exactly how nanofluids influence to heat exchange is not known, there have been major developments in nanofluid technology during the past two decades (2007). Most scientists believe that nanofluids can raise the heat transfer rate. A nanofluid is a fluid containing nanometer-sized particles, called nanoparticles. Nanofluids are nanotechnology based heat transfer fluids in which nanometer-sized particles (generally with a length raging from 1 to 100nm) are suspended. Since most of the conventional fluids have poor thermal properties, nanofluids technology has a great potential to improve this situation.

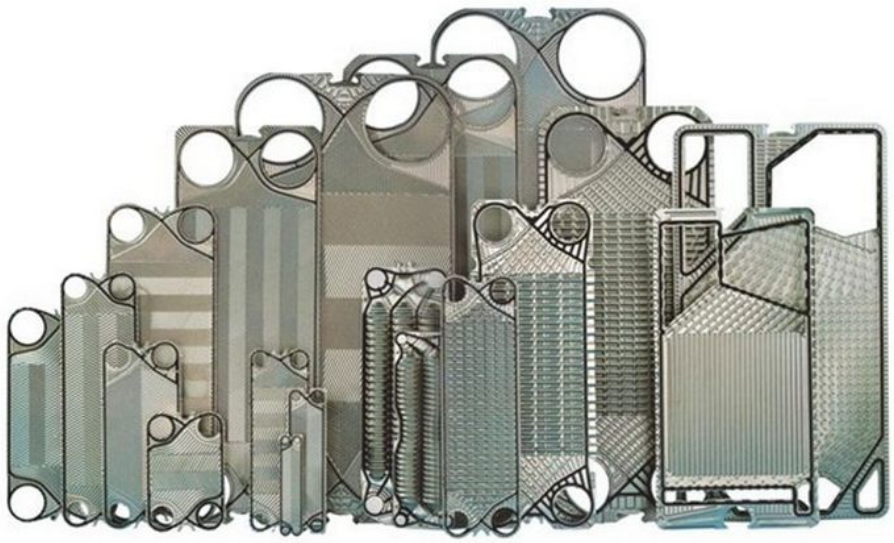

Fig. 1.1 Different kinds of chevron plate

B. Previous studies

Okada et al. (1972) studied the effects of the chevron angle on the Nusselt number and pressure drop at angles of 30°, 45°, 60°, and 75°. Chisholm and Wanniarachchi (1992) studied a chevron plate with a chevron angle ranging from 30°~80°, and they correlated the Nusselt number with the different chevron angles. Khan et al. (2010) conducted a study using water as the working fluid and obtained experimental heat transfer data for single-phase flow configurations in a commercial PHE at symmetric angles of 30°/30°, 60°/60°,and mixed 30°/60° chevron angle plates. Their results showed that the chevron angle had a large effect on the heat transfer and that an angle of 60°/60° produced the best heat transfer performance.

Labib and his coworkers (2013) did a numerical investigation on effect of nanofluids in forced convective heat transfer by using FLUENT. They introduced two- phase model, which is a new concept of combined/hybrid nanofluids. Modern technology now allows the fabrication of materials at the nanometer scale and has dramatically reduced the fabrication costs of such materials. Nanoparticles are a class of materials with unique physical and chemical properties compared to those of larger particles of the same material. Examples of nanoparticle materials used in nanofluids are oxide ceramics (alumina oxide [Al_2O_3] and copper oxide [CuO]), nitride ceramics, carbide ceramics, metals, semiconductors, single-, double-, or multi-walled carbon nanotubes, and composite materials, such as nanoparticle core-polymer shell composites. Research has been ongoing to understand how nanofluids can be used to predict the heat transfer performance. Yu et al. (2007) presented experimental research on the thermal conductivity of nanofluids and

heat transfer and theoretical modeling. In this report, when different kinds of nanoparticles were added to different basic fluids, the fluids showed varying abilities to increase the heat transfer performance. Xu et al. (2006) proposed a model for predicting the thermal conductivity of nanofluids by taking into account the fractal distribution of nanoparticle sizes and the Brownian motion of particles in fluid. Their model showed good agreement with experimental data presented by other researchers (2001-2005). In addition, Pelevic and Meer (2012) studied the effective thermal conductivity of nanofluids numerically. Their study focused on microscopic changes within nanofluids during the heat transfer process. They successfully derived the variation in the thermal conductivity of nanofluids when varying concentrations of CuO and Al_2O_3 were used as nanoparticles and water and ethylene glycol were used as the base fluids. In an experimental study, Shive (2012) analyzed the heat transfer and friction factor when nanofluids were used as coolant in a corrugated PHE. They reported better heat transfer characteristics in the nanofluid system compared with a water-water system. Compare to water-water system, the convective heat transfer coefficient is enhanced most, about 11%, for 2vol.% Al_2O_3/water nanofluids.

The lithium bromide (LiBr) solution is one of the most commonly used working fluids in absorption systems because of its extreme hygroscopic character. It has been well accepted as alternative choice to overcome the environmental problems associated with the use of traditional refrigerants: CFCs and HCFCs. Researchers have studied the thermal properties of LiBr solutions at various temperatures and concentrations. Lower measured various thermodynamic and transport properties of LiBr solution for concentrations varying from 0 to 70% weight percent. Mcneely (1988) measured the thermodynamic properties of LiBr-water solutions.

Chua et al. (2000) measured the thermal properties of a LiBr solution at different mass concentrations and temperatures experimentally and theoretically. Kaita (2001) studied the thermodynamic properties of LiBr-water solutions at mass fractions ranging from 40% to 65% and temperatures ranging from 40℃ to 210℃. In addition, Jung et al. (2013) measured the critical heat flux and the boiling heat transfer coefficient of LiBr solution-based binary nanofluids (0vol.% ~0.1vol.% nanoparticles dispersed in a 3 wt%, 7 wt% and 10 wt% LiBr solution). They found that the boiling heat transfer coefficient of the binary nanofluids decreased, whereas the heat flux increased with increasing concentrations of nanoparticles. Kang et al. (2008) measured the vapor absorption rate and the heat transfer rate for a falling film flow of LiBr solution-based binary nanofluids and compared the enhancement in the heat transfer and mass transfer under the same conditions. Although much research (1988-2001) has been conducted on the properties of LiBr solutions and PHE, little research (2009) on PHEs has used a LiBr solution as the working fluid, let alone LiBr solution-based binary nanofluids.

C. Objectives

In this article, equations for the properties of a LiBr solution were derived based on existing data, and the heat transfer performance of LiBr solution-based binary nanofluids in a chevron PHE was simulated based on universally accepted theories and properties (2007). Different kinds of materials, both metallic and nonmatallic materials (Al_2O_3, Cu and MWCNT), are used as nanoparticles. The volume concentration of nanoparticles and the angles of the chevron plate were changed, and the effects on the variation on the heat transfer rate, the overall heat transfer coefficient, and the effectiveness were then studied using a theoretical method. The effectiveness of the PHE is defined as a ratio of the actual heat transfer rate to the maximum possible heat transfer rate. By comparing the previously mentioned data, the optimal volume fraction for a specified nanoparticle in a PHE can be determined. And the reasons why different nanoparticles lead to different heat transfer performance in PHE are discussed.

Ⅱ. Modeling and verification

A. Development of formulas for the properties of LiBr

In this study, the heat transfer of a specific PHE with different chevron angles was analyzed. In this simulation, LiBr solution containing Al_2O_3 nanoparticles was used as the working fluid. Before conducting a nanofluid simulation, a simulation based on the LiBr solution must first be conducted. As the solution temperature changes throughout the whole process of heat transfer within a PHE, accurate data are needed on the solution density and the specific heat capacity at varying temperatures and solution concentrations. Although much research has been done on LiBr solutions, no firm correlation has been established for variation in the thermal properties of LiBr solutions with temperature and solution concentration. Using experimental data of Chua et al. (2000), the variation in the solution density and specific heat capacity of a LiBr solution versus the temperature and concentration was studied. As shown in Figure 1(a) and (b), based on the discrete experimental data of Chua et al. (2000), the solution density and specific heat capacity value surface were formed, so that any value of specific heat capacity and solution density can be obtained in the range of given conditions. With an increase in the solution temperature, the solution density decreased gradually, and the specific heat capacity showed a slight increase. Conversely, the density increased with the addition of LiBr, and the specific heat capacity rapidly decreased.

Since the solution density and specific heat capacity value have been obtained, then we need to fit these two surfaces by using a fitting equation. In

this study, a rational equation was used as a fitting equation, which can be expressed as follows:

$$Z = \frac{Z_0 + A_{01}x + B_{01}y + B_{02}y^2 + B_{03}y^3}{1 + A_1x + A_2x^2 + A_3x^3 + B_1y + B_2y^2} \quad (1)$$

where Z refers to the solution density or specific heat capacity and A_{01}, A_1, A_2, A_3, B_{01}, B_{02}, B_{03}, B_1 and B_2 are constants.

The solution density and the specific heat capacity can be expressed as:

$$\rho = \frac{1006.66 - 0.968T - 6.99c + 0.0326c^2 - 0.00127c^3}{1 - 5.41\times10^{-4}T + 1.031\times10^{-7}T^2 + 4.136\times10^{-10}T^3 - 0.0127c + 3.854\times10^{-6}c^2} \quad (2)$$

$$c_p = \frac{4.14 - 0.045c + 0.0111T - 6.929\times10^{-5}T^2 + 1.257\times10^{-7}T^3}{1 + 0.0058c - 1.239\times10^{-4}c^2 + 7.24\times10^{-8}c^3 + 0.0021T - 1.029\times10^{-5}T^2} \quad (3)$$

where c is the solution concentration and T is the solution temperature.

As shown in Figures 2.1 and 2.2, the blue wire frame surfaces are well covered by the red wire frame surfaces. In addition, the standard errors for both surfaces are less than 1%.

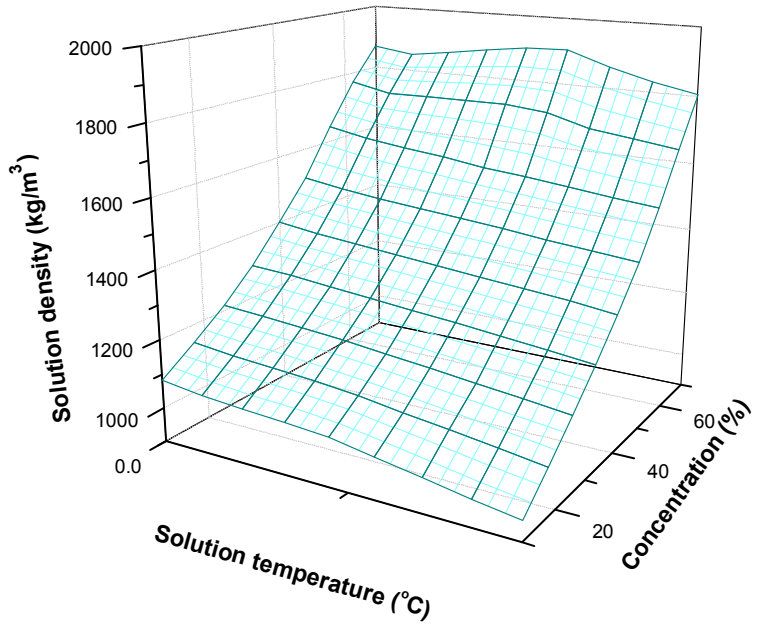

Fig. 2.1 Density of LiBr solution

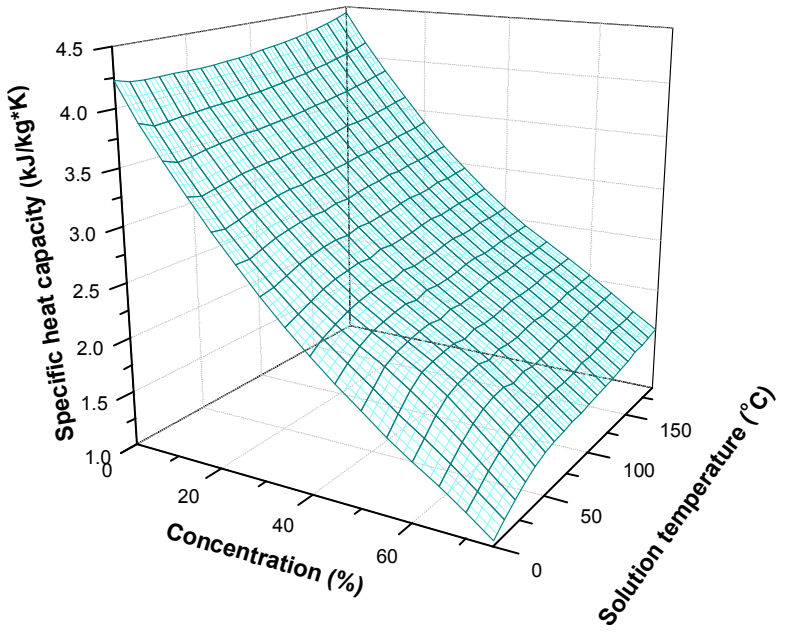

Fig. 2.2 Specific heat capacity of LiBr solution

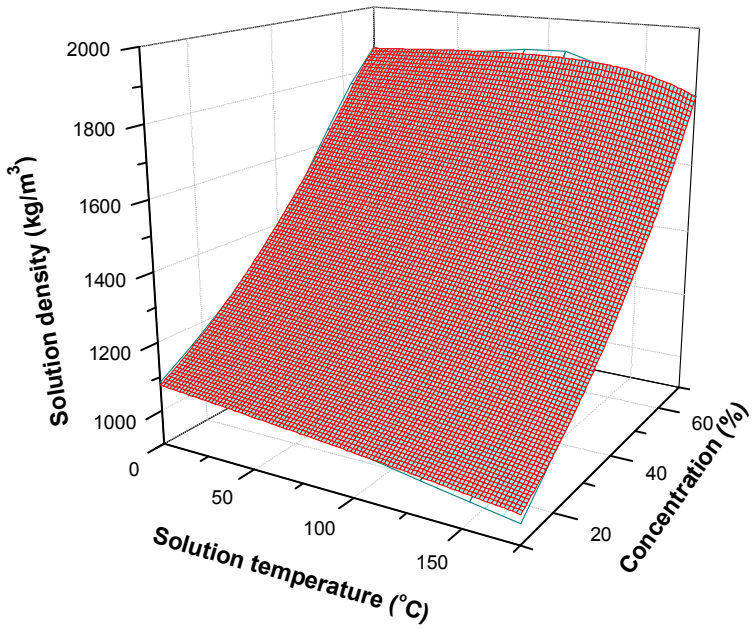

Fig. 2.3 Surface fitting for LiBr solution density

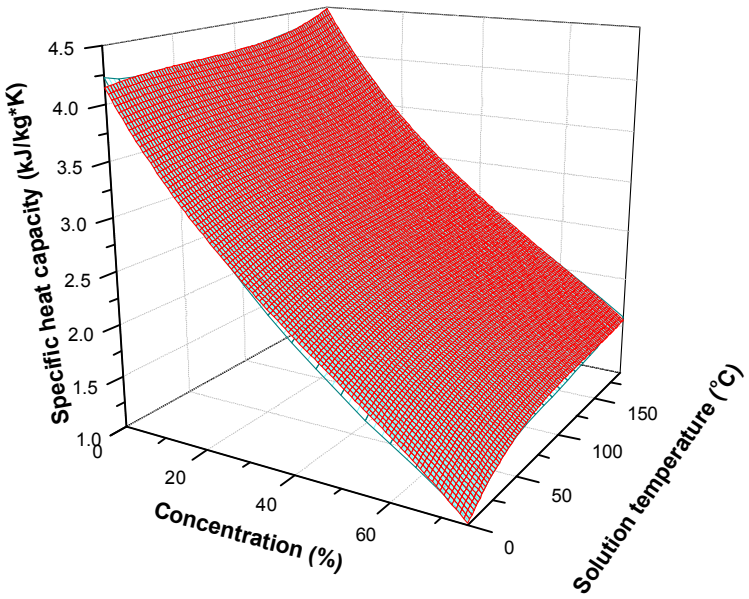

Fig. 2.4 Surface fitting for LiBr solution specific heat capacity

B. Verification of the proposed equations

Kwon et al. (2009) conducted an experimental study of the heat transfer performance of a LiBr solution in PHEs with chevron angles of 30°/30°, 60°/60°, and 30°/60° (mixed) and proposed Nusselt number correlations for the specific chevrons angles. To verify the validity of the equations proposed in the last section, which presented formulas for the solution density and the specific heat capacity, the Nusselt number used in Kwon's study was employed in the simulation. The correlations were as follows:

$$Nu = 1.078\,\mathrm{Re}^{0.403}\,\mathrm{Pr}^{0.333} \tag{4}$$

when the chevron angle was 30°/30° and

$$Nu = 5.194\,\mathrm{Re}^{0.387}\,\mathrm{Pr}^{0.333} \tag{5}$$

when the chevron angle was 60°/60°.

For a 30°/60° PHE, in which 30° plate and 60° plate are mixed installed, the correlation was determined using the data on the Nusselt number in this paper. The correlation was as follows:

$$Nu = 3.2\,\mathrm{Re}^{0.4}\,\mathrm{Pr}^{0.333} \tag{6}$$

The schematic of a PHE is shown in Figure 2.5, and the main parameters of the heat exchanger are shown in Table 2.1. It is not easy to simulate the heat transfer in 30°/60° PHE, thus the hydraulic diameter and geometry heat transfer area was calculated using 45°/45° PHE instead of using a 30°/60° PHE like other researches (2010). In addition, the operating conditions for simulation are shown in

Table 2.2. The value marked with "*" refers to a basic condition, which means that when the mass flow rate of one side of the fluid changes, the mass flow rate at the other side remains constant at the marked value.

Table 2.1 Specification of chevron plate

Item	Specification
Plate size (mm×mm×mm)	289×119×48.8
Corrugation depth, b (mm)	2.0
Plate thickness, t (mm)	0.3
Corrugation pitch, λ (mm)	6.0
Chevron angle, β	30°/30°, 30°/60°,60°/60°

Table 2.2 Test and simulation conditions of working fluid

Item	Hot fluid	Cold fluid
Inlet concentration (wt%)	62.5	58.5
Inlet temperature (℃)	155	70
Solution mass flow rate (kg/h)	150, 250, 350*, 450, 550	340, 360, 380*, 400, 420

*Basic conditions

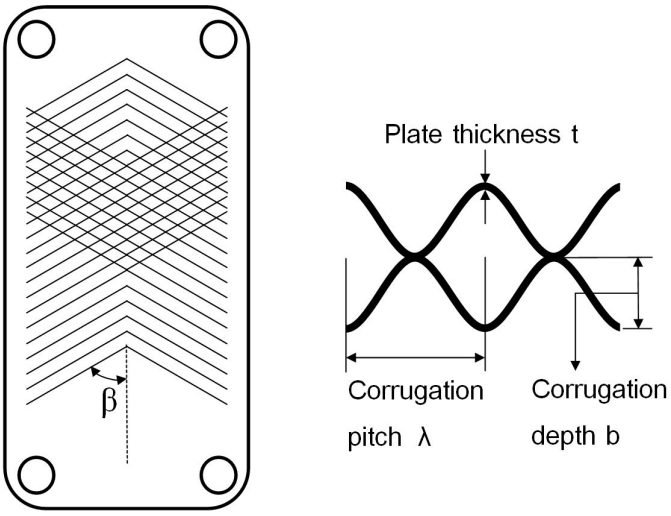

Fig, 2.5 Schematic of chevron plate

C. Nanofluids simulation

Over the past two decades, nanofluid technology has been developing rapidly. Most researchers agree that its thermal performance can be improved by adding nanoparticles to the fluid (2007). especially for fluids that have poor thermal performance, such as water and ethylene. Exactly how nanoparticles improve the thermal performance of fluids is not known clearly. Researchers have focused extensive efforts on understanding the variation in the thermal properties of fluids after adding different kinds of nanoparticles (2007).

A nanofluid can be defined as a mixture consisting of a continuous base fluid component and a discontinuous solid component. The properties of nanofluids, especially their thermal conductivity and viscosity, strongly depend on the microstructure of the fluid (2007). It is impossible at present to estimate the effectiveness of nanofluids unless all the details of their microstructures are known. In the absence of adequate data, a basic assumption is made that a nanofluid is a homogeneous fluid with effective properties.

The effective density and the specific heat capacity of nanofluids can be evaluated by applying the following equations proposed by Pak and Cho (1998):

$$\rho_{nf} = (1-\upsilon_p)\cdot\rho_{bf} + \upsilon\cdot\rho_p \tag{7}$$

$$C_{p_{nf}} = (1-\upsilon_p)\cdot C_{p_{bf}} + \upsilon_p\cdot C_{p_p} \tag{8}$$

These were validated to produce an error within 5% when compared to the experimental data. The effective viscosity can be evaluated using different existing formulas. One of the most widely applied equations is the well-known Einstein’s equation (1998):

$$\mu_{nf} = (1+2.5\upsilon_p)\cdot\mu_{bf} \tag{9}$$

This was shown to be valid for nanofluids with a nanoparticle volume concentration less than 2%. This equation was extended by Brinkman for nanofluids with a volume fraction less than 5% (1952):

$$\mu_{nf} = \frac{\mu_{pf}}{(1-\upsilon_p)^{2.5}} \tag{10}$$

Eqs. (7) and (8) are based on the classical theory of mixtures (1998). Eqs. (7) and (8) have been used in several studies (2011-2013). Eq.(10), which was used to calculate the viscosity of nanofluids containing a dilute suspension of small rigid spherical particles, was suggested by Pelevic and Meer (2012).

As mentioned previously, the properties of nanofluids strongly depend on the microstructure of the nanoparticles that they contain. To evaluate their thermal conductivity, empirical formulas are usually used, but these do not give reliable results (2013). In this study, a LiBr solution with 1%, 2%, 3%, and 4% volume fraction of Al_2O_3 particles, which have an average diameter of 30 nm, was used as the working fluid. The operating conditions for the simulation of the nanofluid are shown in Table 2.2. In the simulation, when the mass flow rate of the hot fluid was used as the variable, the mass flow rate of the cold fluid was constant at 380 kg/h. When the mass flow rate of the cold fluid was employed as the variable, the mass flow rate of the hot fluid kept constant at 350 kg/h. The thermal conductivity was calculated according to the experimental study of Pelevic and Meer (2012) who compared numerical results to experimental results and obtained a good agreement error less than 10%.

For the pressure drop in the PHEs, Xuan and Roetzel (2000) reported that nanofluids showed a great potential in increasing heat transfer rates with incurring either little or no penalty in pressure drop. Likewise, Kalteh et al. (2011) carried out numerically simulation for nanofluids performance in a microchannel and they reported that the pressure drop increasef slightly with increase of the

nanoparticle volume concentration for all Reynolds numbers. For instance, for Re=1000 and volume fraction is 0.01, the percentage increase in pressure drop in comparison to base fluid is 1.99%. In addition, Jung et al. (2013) studied Al_2O_3-water nanofluids in rectangular microchannels, they reported a slight increment in friction factor loss with increasing nanoparticle concentration, which almost could be neglected, that means that the pressure drop increased slightly compared to the base fluid. Overall, in the open literatures, many of them provide reasonable basis that the addition of nanoparticles effects pressure drop little. Given all this, it is reasonable to think that the pressure drop of nanofluids would not bring significant impact on evaluating the performance of the PHEs in the comparison to the PHEs using LiBr solution.

Modern fabrication technology allows the fabrication of materials at the nanometer scale. In order to get well dispersed nanofluid, nanoparticles are most commonly produced in the form of powders by physical or chemical techniques. In this work, alumina, copper and MWCNT nanoparticles are added to the matrix respectively to form a two phase working fluid. Alumina and copper are the first to be used as nanoparticle materials. And MWCNT, that is multi wall carbon nanotube, is allotrope of carbon with a cylindrical nanostructure. Nanotubes have been constructed to have a large length-to-diameter ratio which is up to 132,000,000:1, significantly larger than for any other material. These cylindrical carbon molecules have unusual properties, which are valuable for nanotechnology, electronics, optics and other fields of materials science and technology. In particular, owing to their extraordinary thermal conductivity and mechanical and electrical properties, they are considered to have a great potential to enhance heat transfer performance.

The thermophysical properties of the nanoparticles used in this work are assumed to be constant as shown in Table 2.3. Nanofluid with 0vol.% to 4vol.% copper or alumina nanoparticles are studied. Since if the matrix contains over

0.24vol.% of MWCNT, the fluid would become unstable, 0vol.% to 0.24vol.% MWCNT would be added to the matrix.

Table 2.3 Thermophysical properties of nanoparticles

Property	Al_2O_3	Cu	MWCNT
C_p (J/kg·K)	205	383	702
ρ (kg/m^3)	3970	8954	1800
k (w/m·k)	7.2	400	1500

D. Heat transfer performance analysis

In the present work, to evaluate the performance of the PHE with various chevron angles, the heat transfer rate, the heat transfer coefficient, and the effectiveness of the PHE were calculated according to the following equations:

$$Q = m_h \cdot C_{\mathrm{p},h} \cdot \Delta T_h \tag{10}$$

$$U = \frac{1}{\left(\frac{1}{h_h} + \frac{1}{h_c} + \frac{t}{k_m}\right)} \tag{11}$$

$$\varepsilon = \frac{m_h \cdot C_{p_h} \cdot (T_{h,i} - T_{h,o})}{(m \cdot C_p)_{\min} \cdot (T_{h,i} - T_{c,i})} \tag{12}$$

Besides, the heat capacity rate ratio is defined as the ratio of the smaller to larger heat capacity rate for the two fluid streams, and it can be expressed as:

$$C^* = \frac{(m \cdot C_p)_{\min}}{(m \cdot C_p)_{\max}} \tag{13}$$

Ⅲ. Results and discussion

A. Heat transfer characteristics of the PHE and verification of LiBr solution properties

1. Heat transfer performance with varying mass flow rate of hot fluid

a. Variation of heat transfer rate

By adapting Eqs. (2-6) under the operating conditions were shown in Table 2.2, the heat transfer performance of PHE was simulated. The comparison of the experimental and computational heat transfer rate, the overall heat transfer coefficient, and the effectiveness of the PHE according to solution mass flow rate of the hot fluid are shown in Figure 3.1. The heat transfer rate for both the experimental results and the simulation results tended to increase with the rise in the mass flow rate of the hot fluid. The heat transfer rate increased in the $60^{o}/60^{o}$ and the $30^{o}/60^{o}$ PHE significantly compared to that in the $30^{o}/30^{o}$ PHE. The increase in the heat transfer rate is due to the increase in the mass flow rate and the chevron angle, which has a positive effect on the heat transfer rate by enhancing the fluid turbulence. When the mass flow rate of the hot fluid was 350 kg/h, the heat transfer rate of the $60^{o}/60^{o}$ chevron angle PHE was 18.3% higher than that of the $30^{o}/60^{o}$ PHE and 106.8% higher than that of $30^{o}/30^{o}$ PHE. When the mass flow rate increased from 150 kg/h to 550 kg/h, the heat transfer

rate increased by 68.8%, 110.0%, and 136.9% for the $30^{o}/30^{o}$, $30^{o}/60^{o}$, and $60^{o}/60^{o}$ chevron angle PHEs, respectively. Comparison of the simulation results with the experimental results revealed a good agreement, with errors ranging from -12% to 11%. Most of the data, especially for $30^{o}/30^{o}$ and $60^{o}/60^{o}$ PHEs, had a margin of error of ±4%. The biggest error (-12%) were observed in the $30^{o}/60^{o}$ PHE when the mass flow rate of the hot fluid was 250 kg/h.

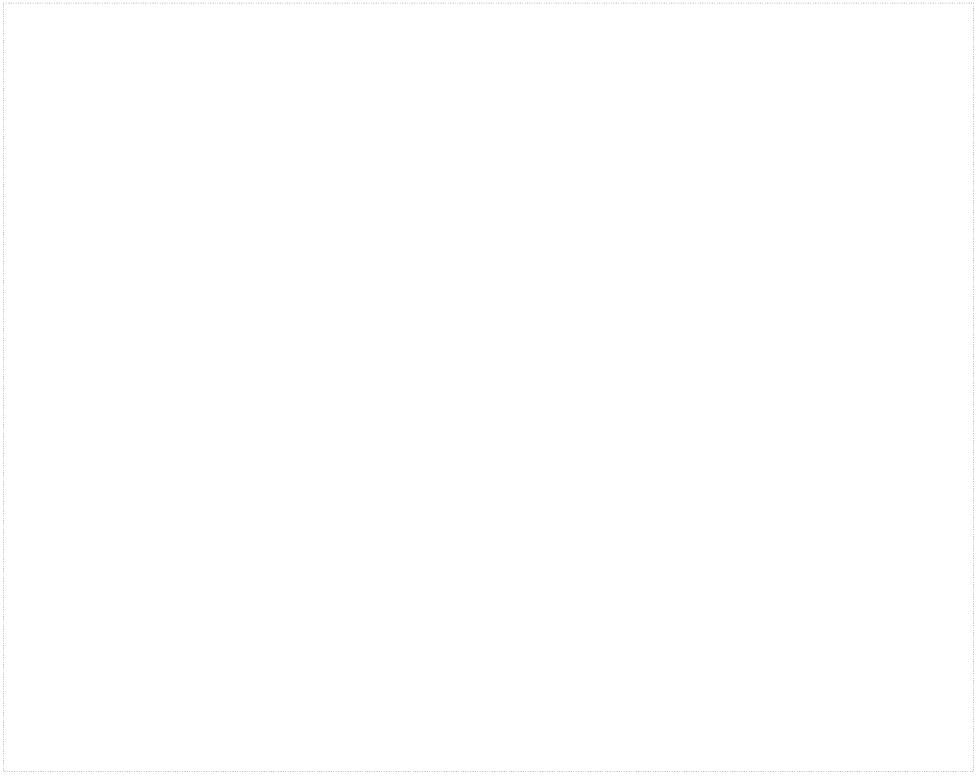

Fig. 3.1 Comparison of experimental and computational heat transfer rate with mass flow rate of hot fluid

b. Variation of overall heat transfer coefficient

Figure 3.2 shows the comparison of the experimental and computational overall heat transfer coefficient with varying solution mass flow rates of hot fluid. Excluding the $30^{o}/60^{o}$ PHE, the simulation results agreed well with the experimental results, with absolute average errors within $\pm 8\%$. For the $30^{o}/60^{o}$ PHE, the error maximum was around 25% for the various mass flow rate of the hot fluid. The error is due to a complex channel that formed in the mixed PHE compared to that of the symmetric PHE. The use of some design factor of $45^{o}/45^{o}$ PHE which is widely employed in commercial PHE leads to the consequence that the fluid flow cannot be reflected perfectly. Overall, the heat transfer coefficient for both the experimental and the simulation results increased gradually with the increase in the mass flow rate of hot fluid for all three cases, with the $60^{o}/60^{o}$ PHE producing the largest value. The higher heat transfer coefficient with the $60^{o}/60^{o}$ PHE is due to the active flow eddy within the channel of the PHE, and it becomes stronger with an increase in the chevron angle and the mass flow rate. Thus, higher heat transfer between the cold and the hot fluid was occurred, resulting in a higher heat transfer coefficient.

Fig. 3.2 Comparison of experimental and computational overall heat transfer coefficient with mass flow rate of hot fluid

c. Variation of effectiveness of PHE

The comparison of the experimental and the computational results of the effectiveness of the PHE were shown in Figure 3.3. The effectiveness of PHE decreased with an increase in the mass flow rate and an increase in the chevron angle. The decrease of effectiveness is due to the maximum possible heat transfer rate being equal at a certain mass flow rate. Thus, heat transfer is more active in high-chevron angle PHEs, and they have a larger actual heat transfer rate. Thus, their effectiveness increases with the chevron angle. In addition, with an increase of the mass flow rate, the amount of the increase in total possible transferred heat is larger than actual transferred heat, resulting in a decrease in the effectiveness of the PHE. The computational data are in good agreement with the experimental results, with the errors around 10% in general. Overall, the simulation results had a similar trend with the experimental results and the error may be acceptable to predicted heat transfer in various operating conditions in the PHE.

According to kwon' s study, the pressure drop in the PHEs increased slightly with the increasing mass flow rate, the average pressure drop for $30^{o}/30^{o}$, $30^{o}/60^{o}$, and $60^{o}/60^{o}$ is 0.35 kPa, 0.6 kPa and 0.7 kPa, respectively. Although the pressure drop in $60^{o}/60^{o}$ PHE is 200% of that in $30^{o}/30^{o}$ PHE, the value of pressure drop are quite small compared to the operational pressure.

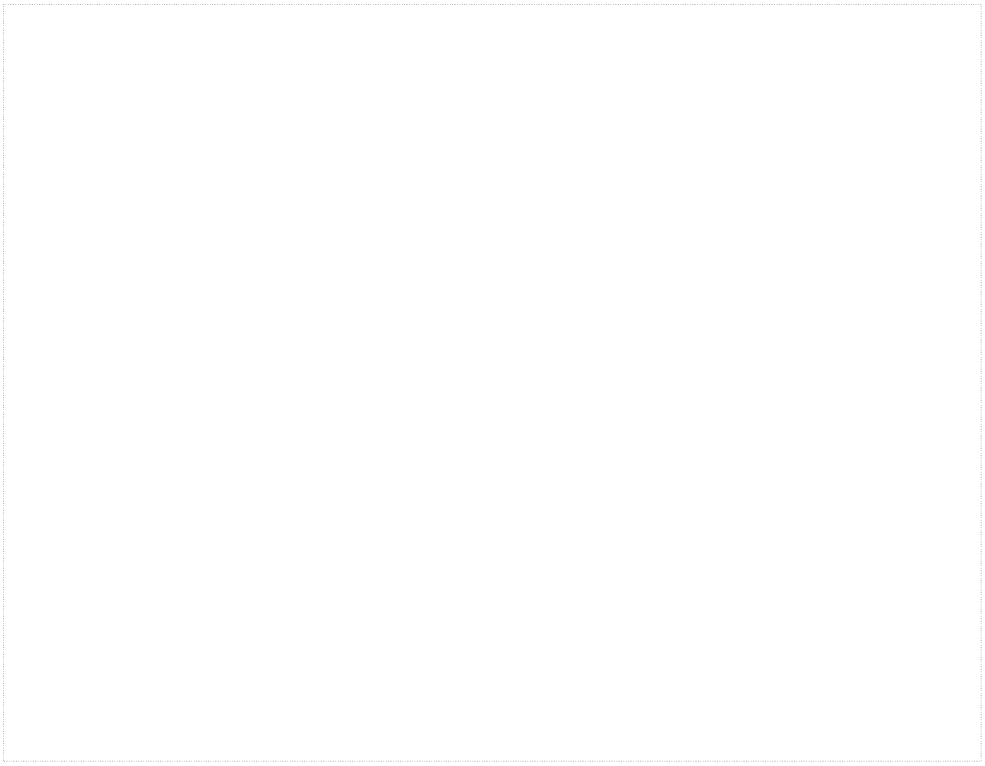

Fig. 3.3 Comparison of experimental and computational effectiveness of the PHE with mass flow rate of hot fluid

2. Heat transfer performance with varying mass flow rate of cold fluid

a. Variation of heat transfer rate

The simulation results of the heat transfer rate of the mass flow rate of the cold fluid and the effectiveness are shown in Figure 3.4. The heat transfer rate and the effectiveness of the PHE tended to increase with a rise in the mass flow rate of the cold fluid. The average heat transfer rate of the $30^{o}/30^{o}$ chevron angle PHE was 5.3 kW, the heat transfer rate of the $60^{o}/60^{o}$ chevron angle PHE was 106.7% higher, on average, than that of the $30^{o}/30^{o}$ PHE, besides, the heat transfer rate of the $30^{o}/60^{o}$ chevron angle PHE was 74.5% higher, on average, than that of the $30^{o}/30^{o}$ PHE. The difference in the heat transfer rate is due to the increase in both the mass flow rate and the chevron angle intensifying the collision effect between the working fluid and the chevron plate. Thus, the heat transfer can proceed more efficiently for higher Re and Pr. With regard to the effectiveness of the PHE, it increased with a rise in the mass flow rate of the cold fluid. As defined in introduction section, the value of the effectiveness of the PHE depends on the actual heat transfer rate and the maximum possible heat transfer rate. As the inlet temperature of both the cold and the hot fluid are fixed, and the mass flow rate of the hot fluid is fixed at 350 kg/h, the maximum possible heat transfer rate is fixed. With an increase in the mass flow rate of the cold fluid, the actual heat transfer rate increases, result in enhancing the effectiveness of the PHE.

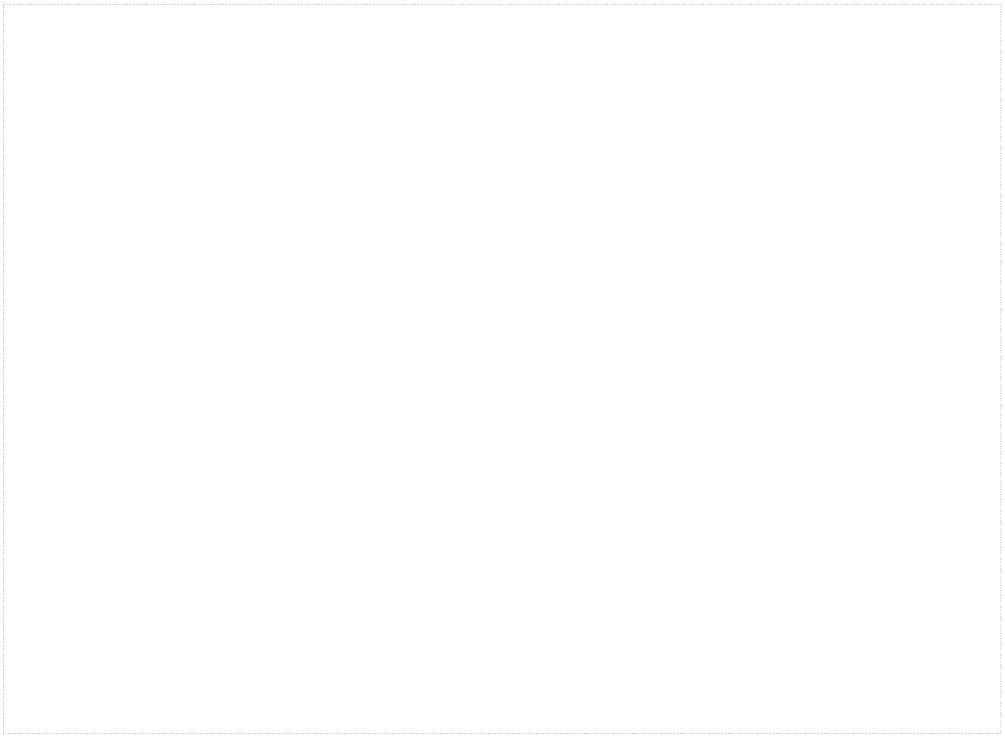

Fig. 3.4 Simulation results of heat transfer rate and effectiveness of the PHE with mass flow rate of cold fluid

b. Variation of overall heat transfer coefficient

Figure 3.5 shows the variation of the heat transfer coefficient according to the mass flow rate of the cold fluid. The heat transfer coefficient increased slowly with an increase in the mass flow rate. The heat transfer coefficient in the $60^{o}/60^{o}$ PHE and $30^{o}/60^{o}$ PHE was 452.2% and 211.6% higher, on average, than that of the $30^{o}/30^{o}$ PHE because of the enhancement of the vortex strength, which was produced by the increase in the mass flow rate of the cold fluid and the chevron angle. The increase of heat transfer coefficient with mass flow rate of cold fluid are 0.005 $kW/m^{2}\cdot℃$ in $30^{o}/30^{o}$ PHE and 0.027 $kW/m^{2}\cdot℃$ in $60^{o}/60^{o}$ PHE, respectively.

Fig. 3.5 Simulation results of heat transfer coefficient with mass flow rate of cold fluid

B. Analysis of the heat transfer performance of the PHE using Al_2O_3-nanofluids

1. Heat transfer performance with varying mass flow rate of hot fluid

a. Variation of heat transfer rate

It has been demonstrated that the addition of nanoparticles to a base fluid leads to a decrease in the specific heat capacity and an increase in the thermal conductivity (2013). The former implies a decrease in the ability of the working fluid to absorb heat and the latter indicates an increased capacity for transferring heat.

Keeping the mass flow rate of the cold fluid at 380 kg/h, the effect of the mass flow rate of the hot fluid and the nanoparticle concentration on the heat transfer performance of PHEs with different angles were analyzed. The variation in the heat transfer rate for the LiBr solution and the LiBr solution with various Al_2O_3-nanoparticle concentrations are shown in Figure 3.6. We can see that in all three angles the PHE ($30^o/30^o$, $30^o/60^o$ and $60^o/60^o$), the heat transfer rate increased with an increase in the mass flow rate of the hot fluid. Under the same hot fluid mass flow rate, the $60^o/60^o$ PHE had the largest heat transfer rate, and the $30^o/30^o$ PHE had the smallest one because the intensive turbulence generation within the PHE was enhanced with the increase in the chevron angle. Compared with the exchanger containing the LiBr solution as the working fluid, for the $30^o/30^o$ PHE, after adding 1% nanoparticles, the heat transfer rate

increased by 2.8%, on average, for various mass flow rates of the hot fluid. For the $60^{o}/60^{o}$ PHE and the $30^{o}/60^{o}$ PHE, the heat transfer rate increased by 2.6% and 1.6%, on average, respectively, with an increase in the mass flow rate of the hot fluid when the 1vol.% nanoparticle was used. This phenomenon can be attributed to the enhancement of the physical properties, especially the thermal conductivity, of the working fluid. With the increase in the volume fraction of the nanoparticles, the thermal conductivity and the viscosity increased, as a result, and the heat transfer rate increased a little. With increase in volume concentration from 0vol.% to 4vol.%, the heat transfer rate of $30^{o}/30^{o}$, $30^{o}/60^{o}$ and $60^{o}/60^{o}$ PHE increased by 8.8%, 4.7% and 3.4%, respectively. We found that in the $60^{o}/60^{o}$ PHE, the 3vol.% binary nanofluid produced the highest heat transfer rate and that a further increase in the concentration of the alumina nanoparticles resulted in a decrease in the heat transfer rate. As we mentioned previously, the heat transfer rate results from interactions between conductivity and viscosity of nanofluid. It seems that in the $60^{o}/60^{o}$ PHE, with the increase in the nanoparticle concentration, the negative impact of the viscosity overwhelmed the positive impact of the conductivity. Thus, the PHE using the 4vol.% nanofluid showed a lower heat transfer rate than that using the 3vol.% nanofluid.

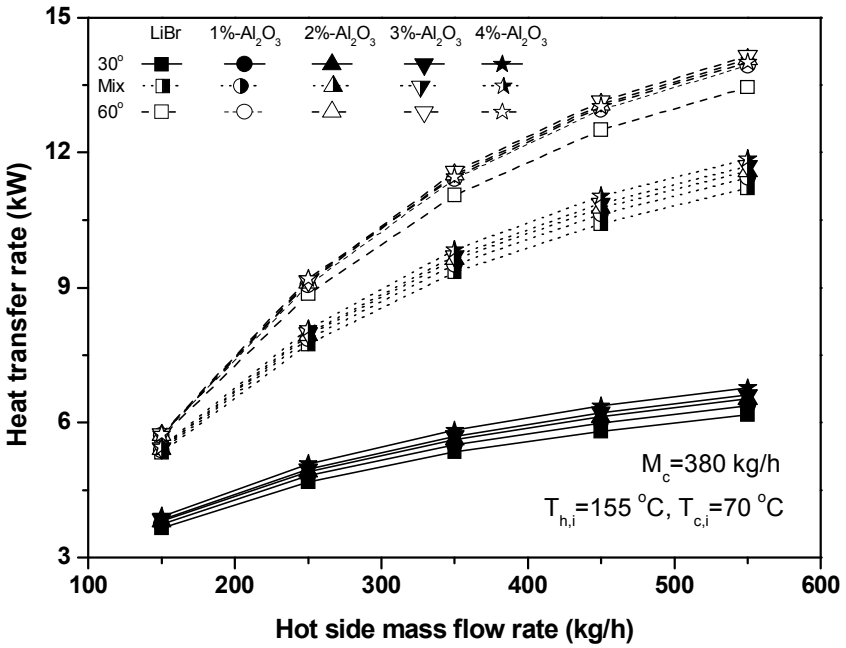

Fig. 3.6 Variation of heat transfer rate for various Al_2O_3-nanofluids concentrations with mass flow rate of hot fluid

b. Variation of overall heat transfer coefficient

The heat transfer coefficient, as shown in Figure 3.7, tended to increase slightly with an increase in the mass flow rate of the hot fluid for all three cases due to the stronger motion of the working fluid within the chevron channel. With increase in volume concentration from 0vol.% to 4vol.%, the heat transfer coefficient of $30^{o}/30^{o}$, $30^{o}/60^{o}$ and $60^{o}/60^{o}$ PHE increased by 15%, 14.9% and 12.8% respectively. Quite similar results were presented in Kabeel' s (2013) experimental study. He reported that compared to the heat transfer coefficient of a base fluid, the heat transfer coefficient of 4vol.% nanofluid was enhanced by 13.0% with an increase in the Reynolds number.

When the LiBr solution was used as the working fluid, for the $30^{o}/30^{o}$ PHE, after adding 1% nanoparticles, the heat transfer coefficient increased by 4.6%, on average, for various mass flow rate of the hot fluid. For the $60^{o}/60^{o}$ PHE, the heat transfer coefficient decreased by 0.2% under the same conditions. For the $30^{o}/60^{o}$ PHE, the heat transfer coefficient increased by 4.8%, on average, with an increase in the mass flow rate of the hot fluid. When the 3% volume fraction of alumina nanoparticles were added to the LiBr solution, the overall heat transfer coefficient increased by 10.8%, 5.5%, and 10.7%, on average, in the $30^{o}/30^{o}$, $60^{o}/60^{o}$, and $30^{o}/60^{o}$ PHEs, respectively. Overall, the heat transfer coefficient increased with an increase in the nanoparticle volume concentration. The increment of the heat transfer coefficient in the $30^{o}/30^{o}$ and $60^{o}/60^{o}$ PHEs was almost the same after adding the alumina nanoparticles. In contrast, the increment in the $30^{o}/60^{o}$ PHE showed less one compare to other cases. According to Shive (2012), the best heat transfer performance was shown at a nanoparticle concentration of 2vol.%, and any further increase in the concentration of the nanoparticles resulted in a decrease in the heat transfer. He reported that with the addition of nanoparticles from 0vol.% to 2vol.%, the viscosity of the working

fluid rapidly increased from 0.798 mPa·S to 2.2 mPa·S (approximately 200%), and the thermal conductivity increased by 1.6%. In addition, the density increased by 1%, and the specific heat decreased by 3.7%. When the volume concentration was increased from 2% to 4%, the viscosity increased by 230%, and the specific heat decreased by 15%, but the thermal conductivity remained almost constant. However, in the present work, the viscosity was calculated by applying Eq. (8), and it increased with similar value, but it did not increase as much as that reported by Shive (2012).

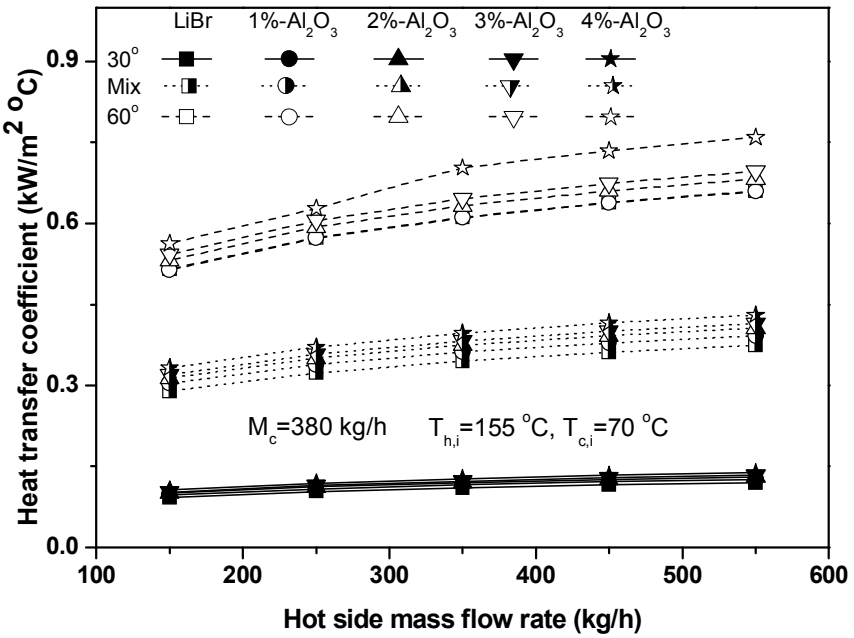

Fig. 3.7 Variation of heat transfer coefficient for various Al_2O_3-nanofluids concentrations with mass flow rate of hot fluid

c. Variation of effectiveness and heat capacity rate ratio

The variations of the effectiveness and the heat capacity rate ratio of the PHE with LiBr solution and the LiBr solution with the nanoparticles are shown in Figure 3.8. For all three kinds of PHE, its effectiveness decreased when the mass flow rate of the hot fluid was increased from 150 kg/h to 450 kg/h. Then it increased when the mass flow rate was further increased to 550 kg/h. By analyzing the process of the heat transfer, it was found that when the mass flow rate increased from 450 kg/h to 550 kg/h, respective fluid side for minimum heat capacity and maximum heat capacity interchanged with each other. As shown in Figure 3.9, with the increase of the mass flow rate, the heat capacity rate ratio increased rapidly at first. Thus, thermal properties of these two fluids tended to be closer, and the effectiveness of the PHE decreased. With a further increase in the mass flow rate, the heat capacity rate ratio decreased, therefore the effectiveness of the PHE increased. This explains the opposite trends observed in the effectiveness of the PHE. In case of 1vol.% nanoparticles, the effectiveness of PHE increased by 2.4% for the $30^{o}/30^{o}$ PHE, on average, for various mass flow rates of the hot fluid compare to that of $30^{o}/30^{o}$ PHE for LiBr solution without nanoparticle. And it was increased by 2.9% for the $30^{o}/60^{o}$ PHE and 2.4% for the $60^{o}/60^{o}$ PHE compare to that of $30^{o}/60^{o}$ and $60^{o}/60^{o}$ PHE for LiBr solution without nanoparticle. With the 2% volume fraction of Al_2O_3, the effectiveness of the PHE increased by 4.2%, 3.0%, and 4.1%, on average, for the $30^{o}/30^{o}$, $60^{o}/60^{o}$, and $30^{o}/60^{o}$ PHEs, respectively. The effectiveness of the PHE increased by 5.2%, 3.3%, and 4.7%, on average, in the $30^{o}/30^{o}$, $60^{o}/60^{o}$, and $30^{o}/60^{o}$ PHEs, respectively, when the 3% volume fraction of alumina nanoparticles were added to the LiBr solution. Overall, the effectiveness of the PHE increased with a rise in the volume concentration of the nanoparticles at the same mass flow rate. When mass flow rate increased from 150 kg/h to 550 kg/h, the average reduction of effectiveness

for three kinds of PHE was 23.8%. Kabeel (2013) also reported that the effectiveness decreased approximately by 25% when Reynolds number increased from 600 to 2000.

Fig. 3.8 Variation of effectiveness of the PHE for various Al_2O_3-nanofluids concentrations with mass flow rate of hot fluid

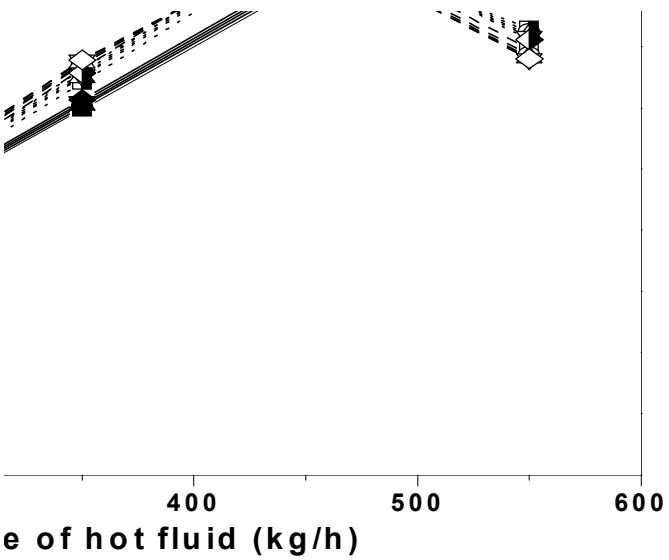

Fig. 3.9 Variation of heat capacity rate ratio for various Al_2O_3-nanofluids concentrations with mass flow rate of hot fluid

2. Heat transfer performance with varying mass flow rate of cold fluid

a. Variation of heat transfer rate

Keeping the mass flow rate of the hot fluid by 350 kg/h, the heat transfer performance of the PHE according to the mass flow rate of the hot fluid and the nanoparticle concentration were investigated. The variations in the heat transfer rate of the PHE for the LiBr solution and the LiBr solution of binary nanofluids are shown in Figure 3.10. The heat transfer rate tended to increase with an increase in the chevron angle and the mass flow rate of the cold fluid because of the enhancement of the vortex strength and flow variety. When the mass flow rate increased from 340 kg/h to 420 kg/h, the heat transfer rate increased by 5.5%, 6.1%, and 5.8%, on average, for the $30^{o}/30^{o}$, $30^{o}/60^{o}$, and $60^{o}/60^{o}$ PHEs, respectively. When the nanoparticle concentration was increased from 0vol.% to 4vol.%, the increment of heat transfer rate in $30^{o}/30^{o}$, $30^{o}/60^{o}$, and $60^{o}/60^{o}$ PHEs were 9.1%, 5.4%, and 3.7%, respectively. Under the same mass flow rate, the heat transfer rate increased with an increase in the nanoparticle concentration in the $30^{o}/30^{o}$ and $30^{o}/60^{o}$ PHEs. This can be attributed to the enhancement of the conductivity of the nanofluids. However, with the increase in the nanoparticle concentration, the heat transfer rate in the $60^{o}/60^{o}$ PHE does not decrease definitely at first, and then decreased. The largest heat transfer rate was obtained at 3vol.% because the viscosity became the dominant factor in the heat transfer after the nanoparticle concentration was larger than 3vol.%.

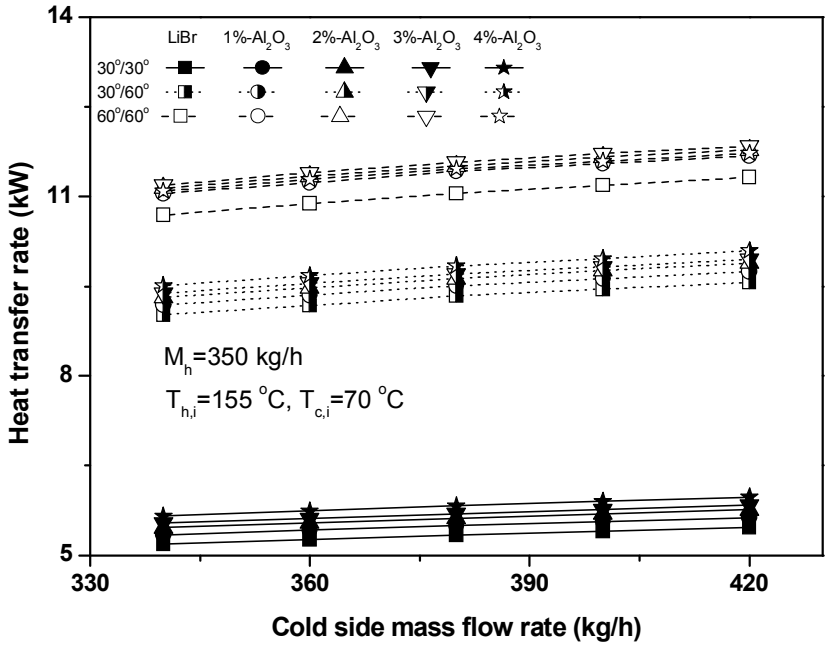

Fig. 3.10 Variation of heat transfer rate for various Al_2O_3-nanofluids concentrations with mass flow rate of cold fluid

b. Variation of effectiveness and heat capacity rate ratio

]The variation of the effectiveness and the heat capacity rate ratio of the LiBr solution and the LiBr solution containing the binary nanofluids is shown in Figures 3.11 and 3.12. The effectiveness of the PHE tended to increase with an increase in the mass flow rate of the cold fluid owing to the decrease in the heat capacity rate ratio. When the mass flow rate increased from 340 kg/h to 420 kg/h, 4.9%, 5%, and 4.7% increases, on average, were obtained for the $30^{o}/30^{o}$, $30^{o}/60^{o}$, and $60^{o}/60^{o}$ PHEs, respectively. When the nanoparticle concentration was increased from 0vol.% to 4vol.%, the increment of effectiveness in $30^{o}/30^{o}$, $30^{o}/60^{o}$, and $60^{o}/60^{o}$ PHEs are 6.9%, 3.8%, and 2.7%, respectively. Similar to the heat transfer rate, for the $60^{o}/60^{o}$ PHE, the largest value was obtained in the 3vol.% binary nanofluids, and any further increase in the nanoparticle concentration leads to a decrease in the effectiveness of the PHE.

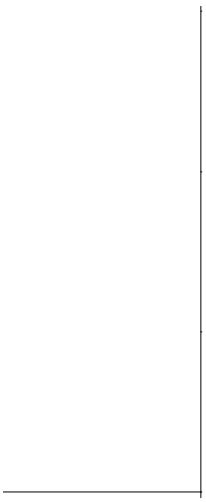

Fig. 3.11 Variation of effectiveness of the PHE for various Al_2O_3-nanofluids concentrations with mass flow rate of cold fluid

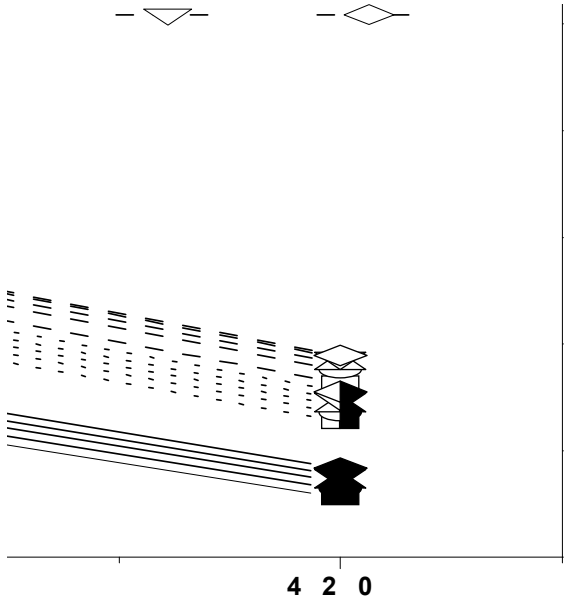

Fig. 3.12 Variations of heat capacity rate ratio for various Al_2O_3-nanofluids concentrations with mass flow rate of cold fluid

C. Analysis of the heat transfer performance of the PHE using Cu-nanofluids

1. Analysis of heat transfer rate

Keeping the mass flow rate of the cold fluid at 380 kg/h, the effect of the mass flow rate of the hot fluid and the copper nanoparticle concentration on the heat transfer performance of PHEs with different angles were analyzed. The variation in the heat transfer rate for the LiBr solution and the LiBr solution with various copper nanoparticle concentrations are shown in Figure 3.13. We can see that in $30^{o}/30^{o}$ PHE, the heat transfer rate increased with an increase in the mass flow rate of the hot fluid, the heat transfer rate of Cu-nanofluid is about 30% higher than that of LiBr solution. The largest value of heat transfer rate is obtained when nanoparticle concentration is 2vol.%, it increased by 31% compared to that of LiBr solution, any further increase in volume concentration leads to a decrease in heat transfer rate.

Gradually, the value of heat transfer rate can be effected by many factors. In nanofluid field, normally, viscosity and thermal conductivity are considered to be quite important. From the previous result, the main reason is that, in low chevron angle PHE, the turbulence is relative mild, thus the increase in viscosity becomes the dominant factor compare to the increase in thermal conductivity. For $30^{o}/60^{o}$ PHE and $60^{o}/60^{o}$ PHE, the heat transfer rate show a similar trend that is it increases with the increase of nanoparticle volume concentration, the maximum value can be got when nanoparticle concentration is 4vol.%, it increased by 20% and 12% respectively. This trend of variation can be attributed to the enhancement of the physical properties, especially the thermal conductivity of the

working fluid. Under the same hot fluid mass flow rate, the 60°/60° PHE had the largest heat transfer rate, and the 30°/30° PHE had the smallest one, and the reason is that the turbulence within the PHE tend to be enhanced with the increase in the chevron angle. With increase in volume concentration from 0vol.% to 4vol.%, the heat transfer rate of 30°/30°, 30°/60° and 60°/60° PHE increased by 30%, 20% and 12%, respectively.

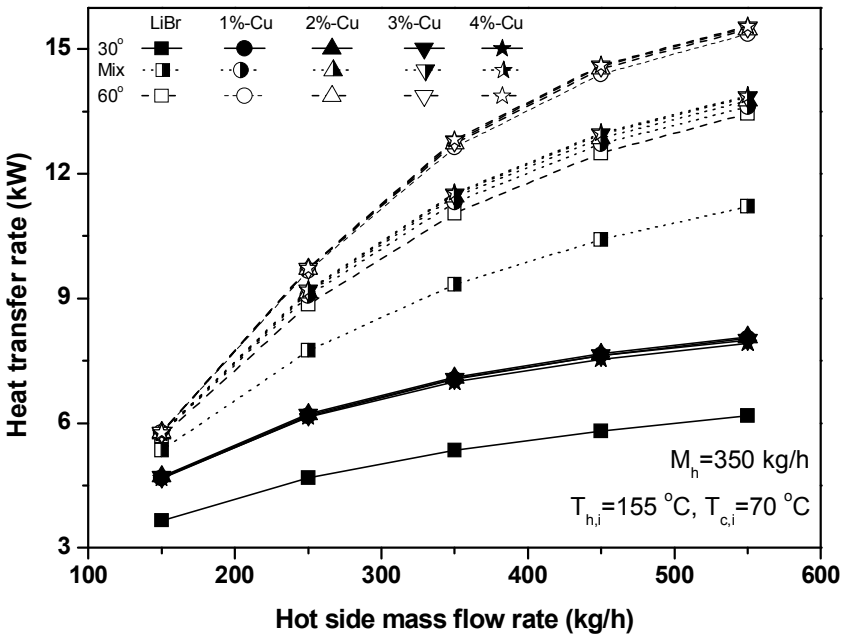

Fig. 3.13 Variation of heat transfer rate for various Cu-nanofluids concentrations with mass flow rate of hot fluid

2. Analysis of heat transfer coefficient

Figure 3.14 shows the variation of heat transfer coefficient. For all three kinds of PHE, the heat transfer coefficient tended to increase slowly with the increase of the mass flow rate of the hot fluid. It is because that a larger flow can bring more intensive turbulence thus the heat transfer process will more active. With the increase in volume concentration from 0vol.% to 4vol.%, the heat transfer coefficient of 30°/30°, 30°/60° and 60°/60° PHE increased by 58%, 92% and 91%, respectively. Compare to the results of Al_2O_3-nanofluid, the heat transfer coefficient of Cu-nanofluid is about 37% higher.

When the LiBr solution was used as the working fluid, for the 30°/30° PHE, after adding 2% nanoparticles, where the maximum heat transfer coefficient can be got, the heat transfer coefficient increased by 61%, on average, for various mass flow rate of the hot fluid. For the 60°/60° PHE, after adding 4% nanoparticles, where the maximum heat transfer coefficient can be obtained, the heat transfer coefficient increased by 91%, on average, for various mass flow rate of the hot fluid. For the 30°/60° PHE, the maximun heat transfer coefficient also can be obtained after adding 4vol.% copper nanoparticles, and it increased by 92%. Overall, the heat transfer coefficient increased with an increase in the mass flow rate. The increment percentage of the heat transfer coefficient in the 30°/60° and 60°/60° PHEs was almost the same after adding the copper nanoparticles. In contrast, the increment in the 30°/30° PHE showed less one compare to other cases.

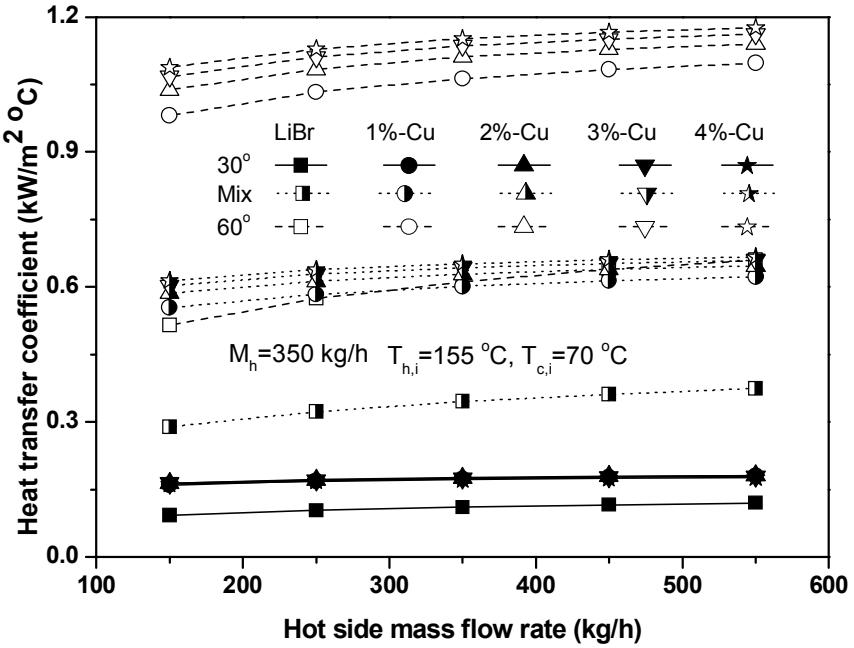

Fig. 3.14 Variation of heat transfer coefficient for various Cu-nanofluids concentrations with mass flow rate of hot fluid

3. Analysis of effectiveness of the PHE

The variations of the effectiveness of the PHE with LiBr solution and the LiBr solution with the copper nanoparticles are shown in Figure 3.15. It can be found from this figure that for all three kinds of PHE, their effectiveness tend to decreased first than increased, although the inflection points are different.

For the $30^{o}/30^{o}$ PHE, after adding 2% nanoparticles, where the maximum effectiveness can be obtained, the effectiveness increased by 0.11, on average, for various mass flow rate of the hot fluid. For the $60^{o}/60^{o}$ PHE, after adding 4% nanoparticles, where the maximum effectiveness can be obtained, the effectiveness increased by 0.13, on average, for various mass flow rate of the hot fluid. For the $30^{o}/60^{o}$ PHE, the maximum effectiveness also can be obtained after adding 4vol.% copper nanoparticles, and it increased by 0.16. Overall, the effectiveness increased with an increase in the mass flow rate. The increment of effectiveness in the $30^{o}/60^{o}$ and $60^{o}/60^{o}$ PHEs was larger than that in the $30^{o}/30^{o}$ PHE.

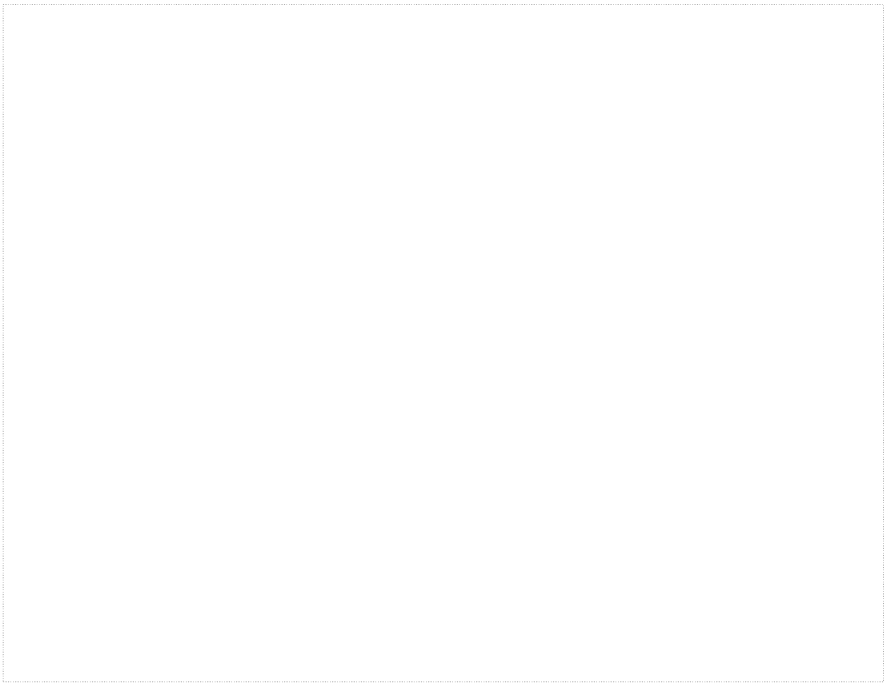

Fig. 3.15 Variation of effectievness for various Cu-nanofluids concentrations with mass flow rate of hot fluid

D. Analysis of the heat transfer performance of the PHE using MWCNT-nanofluids

1. Analysis of heat transfer rate

Keeping the mass flow rate of the cold fluid at 380 kg/h, the effect of the mass flow rate of the hot fluid and the MWCNT nanoparticle concentration on the heat transfer performance of PHEs with different angles were analyzed. The variation in the heat transfer rate for the LiBr solution and the LiBr solution with various MWCNT nanoparticle concentrations are shown in Figure 3.16. We can see that in all three kinds of PHE, the heat transfer rate increased with an increase in the mass flow rate of the hot fluid, also, it increased with an increase in MWCNT volume concentration.

For $30^{\circ}/30^{\circ}$ PHE, the heat transfer rate of MWCNT-nanofluid is about 13% higher than that of LiBr solution. The largest value of heat transfer rate is obtained when nanoparticle concentration is 4vol.%, it is 17% higher than that of LiBr solution on average. For $30^{\circ}/60^{\circ}$ PHE, the heat transfer rate of MWCNT-nanofluid is about 10% higher than that of LiBr solution. The largest value of heat transfer rate is obtained when nanoparticle concentration is 4vol.%, it is 12% higher than that of LiBr solution on average. And for $60^{\circ}/60^{\circ}$ PHE, the heat transfer rate of MWCNT-nanofluid is about 6% higher than that of LiBr solution. The largest value of heat transfer rate is obtained when nanoparticle concentration is 4vol.%, it is 8% higher than that of LiBr solution on average. As mentioned previously, heat transfer rate can be effected by the physical properties, especially the thermal conductivity of the working fluid. There is no any inflection point appeared when MWCNT is used as nanoparticle, the reason is

that compare to alumina and copper, the density and volume fraction of MWCNT is much less and its conductivity is significantly higher, these characteristics make the MWCNT nanofluid get a considerable increase in conductivity and at the same time with no significant increase in viscosity. Under the same hot fluid mass flow rate, the heat transfer rate in the $60^{o}/60^{o}$ PHE had the largest value, and the $30^{o}/30^{o}$ PHE had the smallest one, and the reason is that the turbulence within the PHE tend to be enhanced with the increase in the chevron angle.

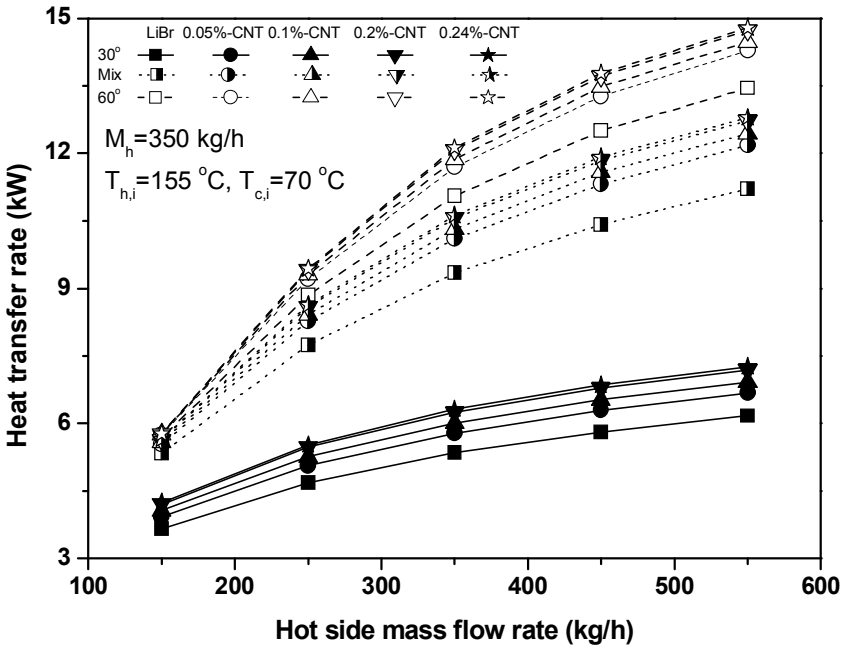

Fig. 3.16 Variation of heat transfer rate for various MWCNT-nanofluids concentrations with mass flow rate of hot fluid

2. Variation of heat transfer coefficient

Figure 3.17 shows the variation of heat transfer coefficient. For all three kinds of PHE, the heat transfer coefficient tended to increase with the increase of the mass flow rate of the hot fluid and it increase faster in high chevron angle PHE because higher chevron angle make the flow in the chevron plate more complicate thus the convective inside the fluid is more active. With the increase in volume concentration from 0vol.% to 4vol.%, the heat transfer coefficient of $30^{o}/30^{o}$, $30^{o}/60^{o}$ and $60^{o}/60^{o}$ PHE increased by 22%, 33% and 33%, respectively. Compare to the results of two former mentioned nanofluids, the heat transfer process in MWCNT-nanofluid is more active that that of Al_2O_3-nanofluid but less active than that of Cu-nanofluid.

It can be observed intuitively that the heat transfer coefficient of nanofluid is much higher than that of LiBr solution for all three kinds of PHE. For all three kinds of PHE, the heat transfer rate increased with an increase in the mass flow rate of the hot fluid and MWCNT volume concentration. When 4vol.% MWCNT-nanoparticles are added to the matrix, that is the LiBr solution, all three kinds of PHE got the largest value of heat transfer coefficient. The heat transfer coefficient increased by 30%, on average, for various mass flow rate of the hot fluid for the $30^{o}/30^{o}$ PHE. For the $30^{o}/60^{o}$ PHE and the $6o0^{o}/60^{o}$ PHE, the heat transfer coefficient both increased by 41%, on average, with an increase in the mass flow rate of the hot fluid. The increment percentage of the heat transfer coefficient in the $30^{o}/60^{o}$ and $60^{o}/60^{o}$ PHEs was almost the same after adding the alumina nanoparticles. The increment in the $30^{o}/30^{o}$ PHE is much smaller.

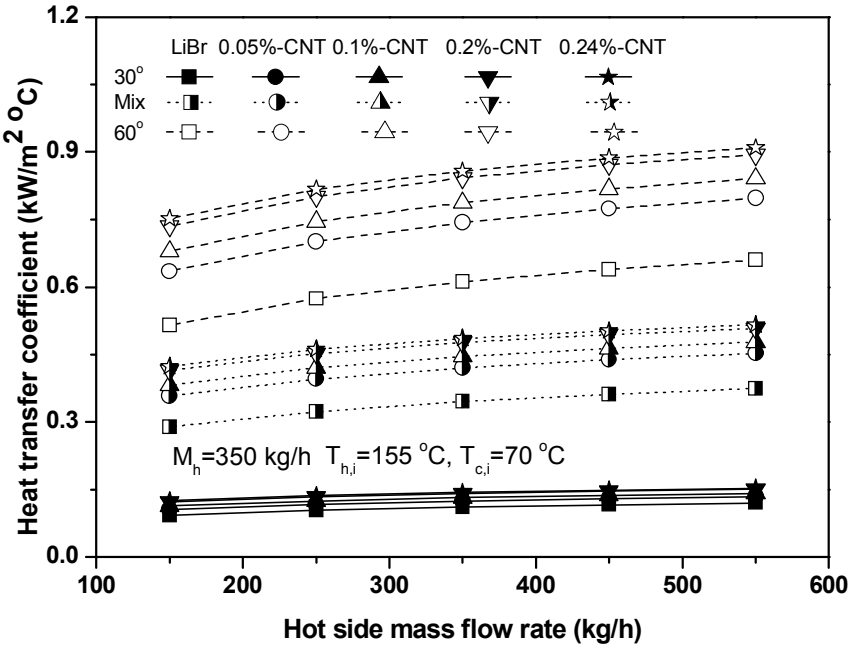

Fig. 3.17 Variations of heat transfer coefficient for various MWCNT-nanofluids concentrations with mass flow rate of hot fluid

3. Analysis of effectiveness of PHE

The variations of the effectiveness of the PHE with LiBr solution and the LiBr solution with the nanoparticles are shown in Figures 3.18. For all three kinds of PHE, its effectiveness decreased when the mass flow rate of the hot fluid was increased from 150 kg/h to 450 kg/h. Then it increased when the mass flow rate was further increased to 550 kg/h.

For all three kinds of PHE, the effectiveness increased with an increase in the mass flow rate of the hot fluid and MWCNT volume concentration. When 4vol.% MWCNT-nanoparticles are added to the matrix, all three kinds of PHE got the largest value of heat transfer coefficient. The effectiveness increased by 0.06, on average, for various mass flow rate of the hot fluid for the $30^{o}/30^{o}$ PHE. For the $30^{o}/60^{o}$ PHE and the $6o0^{o}/60^{o}$ PHE, the effectiveness both increased by 0.08, on average, with an increase in the mass flow rate of the hot fluid. The increment percentage of the heat transfer coefficient in the $30^{o}/60^{o}$ and $60^{o}/60^{o}$ PHEs was almost the same after adding the MWCNT nanoparticles. The increment of effectiveness is smaller compared to that of Cu-nanofluid.

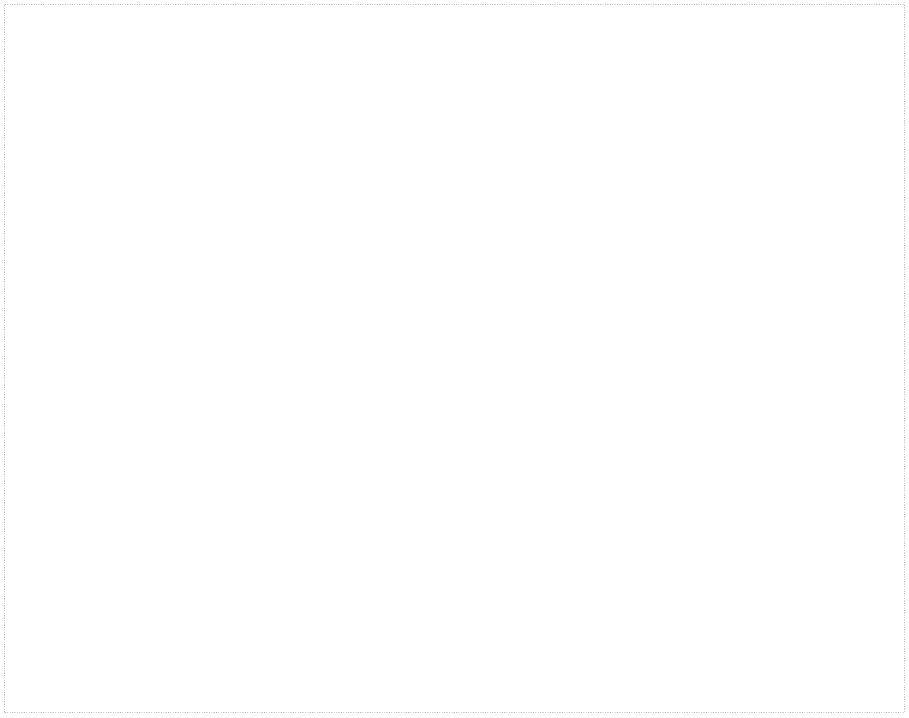

Fig. 3.18 Variation of effectiveness for various MWCNT-nanofluids concentrations with mass flow rate of hot fluid

E. Comparison of the heat transfer performance of the PHE with different nanofluid

1. Comparison of heat transfer rate

For any kind of nanofluid, the largest value of heat transfer rate appear in $60^{o}/60^{o}$ PHE. A comparison of heat transfer rate among the optimum value of nanofluids and LiBr solution is shown in Figure 3.19. A similar variation tendency can be detected from this figure, heat transfer rate increased with the increase of mass flow rate of hot fluid. The deviation between nanofluid and LiBr solution became bigger with the increase of the mass flow rate. That is, the priority of nanofluid can be enhanced with the increase of mass flow rate. Among the four kinds of working fluid, 4vol.% of Cu-nanofluid shows the best heat transfer rate, it is 12% higher than that of LiBr solution. Considering the difficulty of bulk production of Cu nanoparticle powder, it may be not a ideal choice for industrial application. 0.24vol.% MWCNT nanofluid also shows a relative high heat transfer rate, it is 8% higher than that of LiBr solution on average.

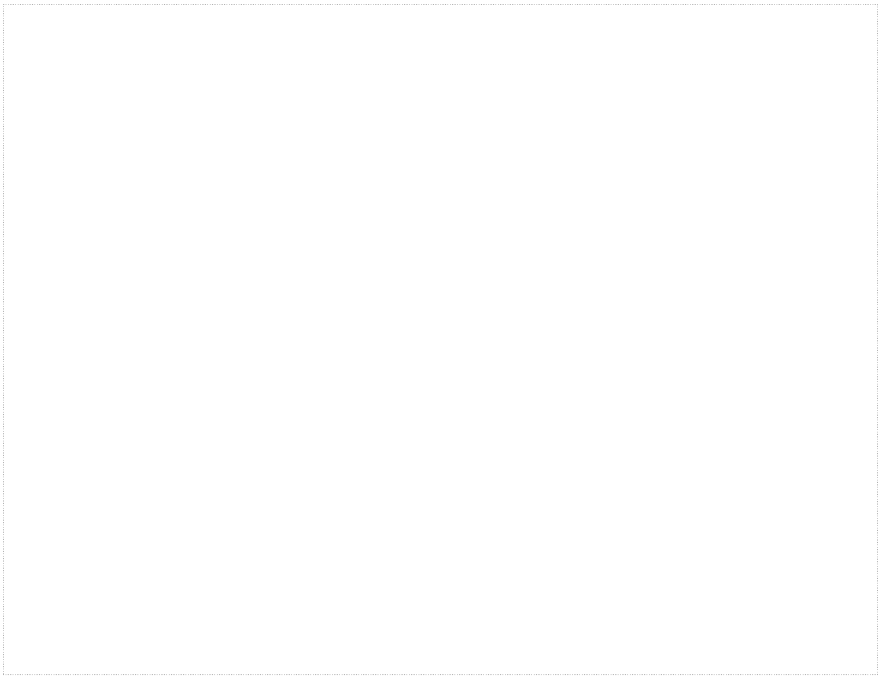

3.19 Comparison of heat transfer rate for different optimal nanofluids with mass flow rate of hot fluid

2. Comparison of heat transfer coefficient

Similar to heat transfer rate, for any kind of nanofluid, the largest value of heat transfer coefficient appear in $60^{o}/60^{o}$ PHE. A comparison of heat transfer coefficient among the optimum value of nanofluid and LiBr solution is shown in Figure 3.20. According to this figure, heat transfer coefficient tend to increase gradually with the increase of mass flow rate of hot fluid and the growth rate for all four kinds of working fluid are almost same. Among the four kinds of working fluid, 4vol.% shows the highest heat transfer coefficient, it is 91% higher than that of LiBr solution. Since bulk production of Cu nanoparticle powder is still not possible and the cost would be increased significantly, it is not suggested in industrial application. 0.24vol.% MWCNT nanofluid also shows a relative high heat transfer rate, it is 41% higher than that of LiBr solution on average. Although MWCNT is still a new kind of nanoparticle material, it is not a hard for bulk production thanks to the advanced manufacture techniques.

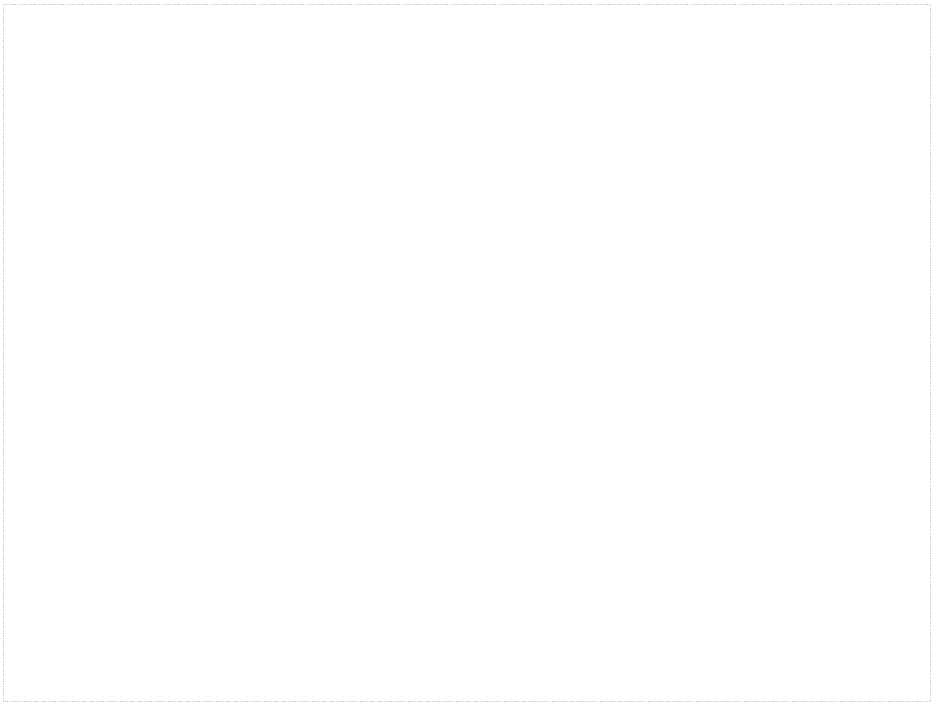

3.20 Comparison of heat transfer coefficient for different optimal nanofluids with mass flow rate of hot fluid

3. Comparison of effectiveness of PHE

A comparison of effectiveness of PHE among the optimum effectiveness of nanofluid and LiBr solution is shown in Figure 3.19. Compared to the variation of heat transfer rate and heat trnasfer coefficient, the variation of effectiveness is more complicated. Overall, 4vol.% Cu nanoparticle showed the largest effectiveness, it is 20% larger than that of LiBr solution. The effectiveness of 0.24vol.% MWCNT nanofluid is 5% larger than that of LiBr solution. And for 4vol.% alumina nanofluid, it got only 3% increment in comparison to that of LiBr solution.

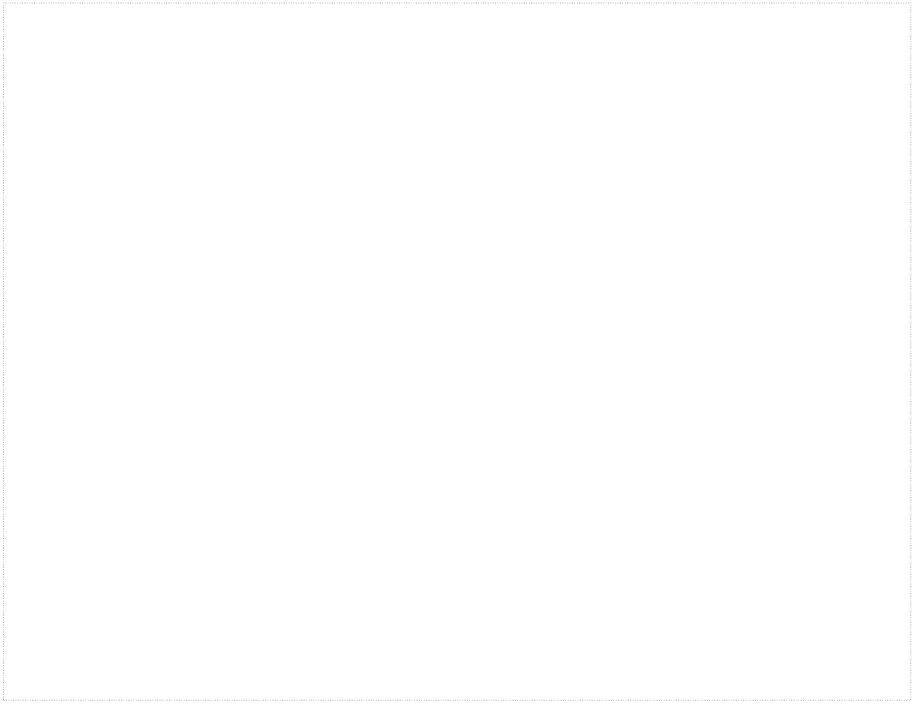

3.21 Comparison of effectiveness of PHE for different optimal nanofluids with mass flow rate of hot fluid

IV. Conclusion

In this study, the heat transfer performance in various chevron angles PHE with LiBr solution-based binary nanofluids were studied numerically. For this, new correlations for the thermo properties of the LiBr solution were firstly derived. By comparing to the experimental data, the correlations are verified to be valid with an error less than 1%.

Besides, the simulation model for heat transfer performance of LiBr solution in chevron PHE was established. The heat transfer rate and the heat transfer coefficient in $60^{\circ}/60^{\circ}$ PHE is over 100% higher than that of $30^{\circ}/30^{\circ}$ PHE, and the effectiveness of the PHE in $60^{\circ}/60^{\circ}$ PHE is about 70% higher than that of $30^{\circ}/30^{\circ}$ PHE. By comparing to the experimental data, most of simulation results of this study were considered to be valid with an error within 10%.

The developed model was used to simulate the heat transfer performance of binary nanofluids (Al_2O_3, Cu and MWCNT) in PHE. By using nanoparticle in the working fluid, the heat transfer performance can increase significantly. The heat transfer rate, heat transfer coefficient, effectiveness and heat capacity rate at different volume concentration of nanoparticles in LiBr solution was investigated.

For alumina nanofluid, when mass flow rate of cold fluid was kept constant, on the basis of $30^{\circ}/30^{\circ}$ PHE with LiBr solution, the maximum increase of heat transfer rate was up to 105% and the maximum increase of effectiveness was up to 92%, both of them can be observed at the concentration of 3vol.%. Under the constant mass flow of hot fluid, the heat transfer rate was increased by 116.5%; the increase of effectiveness of the PHE was increased by 93.7%, both of them can be observed at the concentration of 3vol.%, too. Considering of heat transfer

and effectiveness enhancement, 3vol.% binary nanofluid is the optimal volume fraction for given operation conditions.

For copper nanofluid, when mass flow rate of cold fluid was kept constant, the maximum increase of heat transfer rate was up to 122% and the maximum increase of effectiveness was up to 104% compare to that of $30^{o}/30^{o}$ PHE with LiBr solution, both of them can be observed at the concentration of 4vol.%. And for $30^{o}/30^{o}$ PHE, the maximum increment of heat transfer rate and effectiveness can be detected when nanoparticle fraction is 2vol.%. We can conclude that in $30^{o}/30^{o}$ PHE, 2vol.% Cu nano-powder would be the optimal choice while 4vol% Cu nano-powder would be better for $30^{o}/60^{o}$ and $60^{o}/60^{o}$ PHE.

For MWCNT nanofluid, when mass flow rate of cold fluid was kept constant, the maximum increase of heat transfer rate was up to 113% and the maximum increase of effectiveness was up to 96% compare to that of $30^{o}/30^{o}$ PHE with LiBr solution, both of them can be observed at the concentration of 0.24vol.%.

The heat transfer rate and effectiveness, which are two most typical parameters in evaluating the performance of a PHE, are largest in Cu-nanofluid. However, manufacture of metallic nanoparticles like copper nanoparticle requires a vaccuum significantly slow the production of nanoparticles, thus limitating the rate of production. Furthermore, producing metallic nanoparticles need to prevent oxidation of the particles, the cost of production is more expensive. Overall, MWCNT is the best choice with a relative larger value of heat transfer rate and effectiveness.

Through this study, we can find that metal nanoparticle has a significant advantage in heat transfer performance, however, limited by economic reasons, it can not be widely applied as far. As a new material, MWCNT also has a great

potential in enhancing heat transfer performance, due to the restriction of stability, the use of MWCNT obviously is limited. For metallic nanoparticles like alumina, because of the existence of inflection point, the heat transfer can not be enhanced as much as by MWCNT and alumina, but they are easy to manufacture. So it can be expected that metal nanoparticles are not suitable for conventional use; while MWCNT and metal oxides nanoparticles can be scaled up to wide use.

REFERENCE

A.E. Kabeel, T. Abou El Maaty, Y. El Samadony, 2013, The effect of using nano-particles on corrugated plate heat exchanger performance, Applied Thermal Engineering vol.52, pp.221-229.

A.E. Kabeel, T. Abou El Maaty, Y. El Samadony, 2013, The effect of using nano-particles on corrugated plate heat exchanger performance, Applied Thermal Engineering vol.52, pp.221-229.

C.H Chon, K.D. Kihm, S.P. Lee and S. Choi, 2005, Empirical correlation finding the role of temperature and particle size for nanofluid (Al2O3) thermal conductivity enhancement, Applied Physics Letters vol.87, pp.107-153.

D. Chisholm, A.S. Wanniarachchi, 1992, Maldistribution in single-pass mixedchannel plate heat exchangers, in: Compact Heat Exchangers for Power and Process Industries, American Society of Mechanical Engineers; Heat Transfer Division Series, vol.201, pp.95-99.

Das S K, Putra N, Thiesen P and Roetzel W, 2003, Temperature dependence of thermal conductivity enhancement for nanofluids, Journal of Heat Transfer vol.125 (4), pp.567-574.

H.C. Brinkman, 1952, The viscosity of concentrated suspensions and solution, The Journal of Chemical Physics vol.20, pp.571-581.

H.T. Chua, H.K. Toh, A. Malek, K.C. Ng, K. Srinivasan, 2000, Improved thermodynamic property fields of LiBr-H2O solution, International Journal of Refrigeration vol.23, pp.412-429.

Huaqing X, Jincahng w, Tonggeng X, Yan L, Fei A and Qingren W, 2002, Thermal Conductivity Enhancement Of Suspensions Containing Nanosized Alumina Particles, Journal of Applied Physics vol.91, pp.45-68.

J. A. Eastman, S. U. S. Choi, S. Li, W. Yu and L. J. Thompson, 2001, Anomalously increased effective thermal conductivities of ethylene glycol-based nanofluids containing copper nanoparticles, Applied Physics Letters vol.78, pp.718.

J. Xu, B. Yu, 2006, A new model for heat conduction of nanofluids based on fractal distributions of nanoparticles, Journal of Physics D: Applied Physics vol.39, 4486-4490.

J.D. Marcos, M.Izquierdo, R. Lizarte, E. Palacios, C.A. Infante Ferreira, 2009, Experimental boiling heat transfer coefficients in the high temperature generator of a double effect absorption machine for the lithium bromide/water mixture, International Journal of Refrigeration vol.32, pp.627-637.

J.Y. Jung, E.S. Kim, Y. Nam, Y.T Kang, 2013, The study on the critical heat flux

and pool boiling heat transfer coefficient of binary nanofluids (H2O/LiBr+Al2O3), International Journal of Refrigeration vol.36, pp.1056-1061.

K. Hadad, A. Rahimian, M.R. Nematollahi, 2013, Numerical study of single and two-phase models of water/Al2O3 nanofluid turbulent forced convection flow in VVER-1000 nuclear reactor, Annals of Nuclear Energy vol.60, pp.287-294.

K. Okada, M. Ono, T. Tomimura, T. Okuma, H. Konno, S. Ohtani, 1972, Design and heat transfer characteristics of a new plate heat exchanger, Heat Transfer Japanese Research vol.1, pp.90-95.

M. Kalteh, A. Abbassi, M. Saffar-Avval, J. Harting, 2011, Eulerian-Eularian two-phase numerical simulation of nanofluid laminar forced convection in a microchannel, International Journal of Heat and Fluid flow vol.32, pp.107-116.

M. Mahmoodi, 2011, Numerical simulation of free convection of a nanofluid in L-shaped cavities, International Journal of Thermal Sciences vol.50, pp.1731-1740.

M. Nuim Labib, Md. J. Nine, H. Afrianto, H.S. Chung, H.M. Jeong, 2013,Numerical investigation on effect of base fluids and hybrid nanofluid in forced convective heat transfer, International Journal of Thermal Sciences vol.71, pp.163-171.

McNeely LA., 1988, Thermodynamic properties of aqueous solutions of lithium-bromide water solutions, ASHRAE Transactions vol.94, pp.2379-88.

N. Pelevic, Th.H. van der Meer, 2012, Numerical investigation of the effective thermal conductivity of nano-fluids using the lattice Boltzmann model, International Journal of Thermal Sciences vol.62, pp.154-159.

O.K. Kwon, D.A. Cha, J.H. Yun and H.S. Kim, 2009, Performance evaluation of plate heat exchanger with chevron angle variations, Transition of KSME B vol.33, pp.520-526.

Pak, B.C., Cho, Y.I., 1998, Hydrodynamic and heat transfer study of dispersed fluids with submicron metallic oxide particles, Experimental Heat Transfer vol.11, pp.151-170.

S.D. Pandey, V.K. Nema, 2012, Experimental analysis of heat transfer and friction factor of nanofluid as a coolant in a corrugated plate heat exchanger, Experimental Thermal and Fluid Science vol.38, pp.248-256.

T.S. Khan, M.S. Khan, M.C. Chyu, Z.H. Ayub, 2010, Experimental investigation of single phase convective heat transfer coefficient in a corrugated plate heat exchanger for multiple plate configurations, Applied Thermal Engineering vol.30 pp.1058-1065.

T.S. Khan, M.S. Khan, Ming-C. Chyu, Z.H. Ayub, 2010, Experimental investigation of single phase convective heat transfer coefficient in a corrugated plate heat exchanger for multiple plate configurations, Applied Thermal Engineering vol.30, pp.1058-1065.

Troupe, R. A., Morgan, J. G., & Prifti, J., 1960, The plate heat exchanger - versatile chemical engineering tool, Chemical Engineering Progress vol.56, pp.124-128.

W. Yu, D.M. France, S.U.S. Choi, and J.L. Routbort, 2007, Review and assessment of nanofluid technology for transportation and other applications.

Y. Xuan, W. Roetzel, 2000, Conceptions for heat transfer correlation of nanofluids, International Journal of Heat and Mass Transfer vol.43, pp.3701-3707.

Y.Kaita, 2001, Thermodynamic properties of lithium bromide-water solutions at high temperatures, International Journal of Refrigeration vol.24, pp.374-390.

Y.T Kang, H.J. Kim, K.I. Lee, 2008, Heat and mass transfer enhancement of binary nanofluids for H2O/LiBr falling film absorption process, International Journal of Refrigeration vol.31, pp.850-856.